IMMUNOLOGY

Cellular sensing of extracellular purine nucleosides triggers an innate IFN-β response

Rekha Dhanwani[1]*, Mariko Takahashi[1]*, Ian T. Mathews[1,2,3]*, Camille Lenzi[1], Artem Romanov[1], Jeramie D. Watrous[2,3], Bartijn Pieters[1], Catherine C. Hedrick[1], Chris A. Benedict[1], Joel Linden[1,3], Roland Nilsson[4,5], Mohit Jain[2,3], Sonia Sharma[1†]

Copyright © 2020 The Authors, some rights reserved; exclusive licensee American Association for the Advancement of Science. No claim to original U.S. Government Works. Distributed under a Creative Commons Attribution NonCommercial License 4.0 (CC BY-NC).

Mechanisms linking immune sensing of DNA danger signals in the extracellular environment to innate pathways in the cytosol are poorly understood. Here, we identify a previously unidentified immune-metabolic axis by which cells respond to purine nucleosides and trigger a type I interferon-β (IFN-β) response. We find that depletion of ADA2, an ectoenzyme that catabolizes extracellular dAdo to dIno, or supplementation of dAdo or dIno stimulates IFN-β. Under conditions of reduced ADA2 enzyme activity, dAdo is transported into cells and undergoes catabolysis by the cytosolic isoenzyme ADA1, driving intracellular accumulation of dIno. dIno is a functional immunometabolite that interferes with the cellular methionine cycle by inhibiting SAM synthetase activity. Inhibition of SAM-dependent transmethylation drives epigenomic hypomethylation and overexpression of immune-stimulatory endogenous retroviral elements that engage cytosolic dsRNA sensors and induce IFN-β. We uncovered a previously unknown cellular signaling pathway that responds to extracellular DNA–derived metabolites, coupling nucleoside catabolism by adenosine deaminases to cellular IFN-β production.

INTRODUCTION

Innate immunity is a universal cellular response to pathogenic threats. Upon sensing infection, damage, or genotoxic stress, susceptible cells activate innate immune signaling cascades such as the interferon-β (IFN-β) axis. IFN-β is a pleiotropic cytokine that signals via the type I IFN receptor (IFNAR) to exert autocrine and paracrine effects on cellular growth, apoptosis, and immune cell activation, ultimately playing an essential role in propagation and resolution of the inflammatory response (*1*). IFN-β is produced during the course of infection, neoplastic transformation, cancer immunotherapy, and autoimmune disease due to cellular recognition of atypical or mislocalized nucleic acids, which involves both intrinsic and extrinsic sensing mechanisms (*2*, *3*). Cell-intrinsic RNA or DNA ligands derive from internalized viruses and bacteria or from host-cellular sources such as damaged mitochondria, stalled replication forks, or endogenous retroviral elements encoded within the genome. Inside the cell, these aberrant nucleic acids are recognized by cytoplasmic sensors such as retinoic acid–inducible gene-I (RIG-I), melanoma differentiation–associated protein 5 (MDA5), or cyclic guanosine monophosphate–adenosine monophosphate synthetase (cGAS). Engagement of innate cytosolic sensors in turn activates key signaling adaptor proteins including mitochondrial antiviral signaling (MAVS) or stimulator of IFN genes (STING), which drive IFN-β production.

How extracellular nucleic acids engage cytosolic sensors is incompletely understood. Extracellularly, Mammalian DNA is a damage-associated molecular pattern (DAMP) with immune-stimulatory activity that largely depends recognition by internal sensors (*4*). Specialized phagocytic cells, including monocytes, macrophages, and dendritic cells, may engulf extracellular DNA fragments to access the cytosolic machinery. However, it is unclear how nonphagocytic or stromal cells respond to extracellular DNA danger signals or whether extracellular DNA–derived metabolites generated by the activity of endonucleases and other nucleic acid modifying enzymes can act in an extrinsic or paracrine manner to modulate the innate immune response.

Here, we describe a previously unidentified cellular response to extracellular deoxy-adenosine (dAdo), which stimulates IFN-β and an IFN-β–driven innate immune response in a paracrine manner. We show that loss of extracellular adenosine deaminase 2 (ADA2) enzyme activity in stromal endothelial cells drives increased cellular uptake of extracellular dAdo into stromal endothelial cells. Upon transport into the cell, dAdo is catabolized by the cytosolic isoenzyme ADA1 to yield dIno, which specifically accumulates inside the ADA2-depleted cells. dIno is a functional immunometabolite that perturbs the cellular metabolic reactions suppressing expression of endogenous retroviral elements, immune-stimulatory molecules that directly engage innate cytosolic double stranded RNA (dsRNA) sensors. Our results suggest that metabolism of extracellular DNA or nucleoside danger signals, which are released due to ischemia, infection, and tumor growth, is a key regulatory checkpoint during physiological inflammation. These regulatory mechanisms are likely abolished in human metabolic syndromes such as ADA2 deficiency or purine nucleoside phosphorylase (PNP) deficiency diseases, which manifest as profound immunological dysregulation characterized by systemic inflammation and inappropriate induction of IFN-β and other innate cytokines.

RESULTS

Loss of ADA2 triggers spontaneous IFNβ production

Gene mutations in molecules of the innate cytosolic sensing machinery drive systemic inflammatory diseases in humans due to excessive IFN-β production (*5*). We reasoned that new mechanistic insights into innate immune sensing and molecular triggers of inflammation could be gained by examining functionally uncharacterized disease-associated genes. Search of the Online Mendelian Inheritance in

[1]La Jolla Institute for Immunology, La Jolla, CA 92037, USA. [2]Department of Medicine, University of California, San Diego, La Jolla, CA 92093, USA. [3]Department of Pharmacology, University of California, San Diego, La Jolla, CA 92093, USA. [4]Cardiovascular Medicine Unit, Department of Medicine, Karolinska Institutet, Karolinska University Hospital, SE-17176 Stockholm, Sweden. [5]Center for Molecular Medicine, Karolinska Institutet, Karolinska University Hospital, SE-17176 Stockholm, Sweden.
*These authors contributed equally to this work.
†Corresponding author. Email: soniasharma@lji.org

Downloaded from http://advances.sciencemag.org/ on February 24, 2021

Man database identified 38 syndromes of systemic inflammation each resulting from a single, sequence-verified gene mutation (table S1). To examine whether any of the candidate disease genes regulate IFN-β pathway activation, in situ immunofluorescence was used to assess inducible nuclear translocation of the transcription factor IFN regulatory factor 3 (IRF3) (*6*), which directly transactivates the IFN-β promoter locus. Upon transfection with immune-stimulatory poly (dA:dT) DNA, IRF3 translocation and IFN-β mRNA levels were quantified in primary human umbilical vein endothelial cells (HUVECs) and other endothelial lineage cells (fig. S1, A and B). Forward genetic screening in HUVEC confirmed STING and three prime repair exonuclease I (TREX1), an inhibitor of DNA sensing through STING, as positive and negative regulators of IRF3/IFN-β, respectively. Results identify ADA2 as a new negative regulator of IRF3 activation (Fig. 1A and table S1).

To ascertain whether loss of ADA2 expression drives spontaneous IRF3 activation in the absence of exogenous stimulation, phosphorylation of IRF3 and autophosphorylation of the IRF3 kinase Tank-binding kinase 1 (TBK1) were examined in ADA2 knockdown cells. Western blotting with phospho-specific antibodies demonstrated spontaneous phosphorylation of IRF3 and TBK1 in small interfering RNA targeting ADA2 (siADA2)–treated or small interfering RNA targeting TREX1 (siTREX1)–treated cells compared to a control, nontargeting small interfering RNA (siControl) (Fig. 1B). *IFN*-β mRNA levels were also spontaneously elevated in ADA2-depleted cells (Fig. 1C) and were further enhanced upon infection with human cytomegalovirus (hCMV), a β-herpesvirus that induces a robust cellular IFN-β response (*6*). Induction of an IFN-β–stimulated gene signature in unstimulated siADA2-treated cells was observed using whole-genome transcriptome analysis (Fig. 1D). Differentially expressed transcripts in this dataset included genes encoding proinflammatory cytokines, chemokines, and innate immune response proteins (Fig. 1E). These findings are concordant with previous observations that IFN-associated gene expression signatures are detectable in peripheral blood cells from ADA2-deficient patients (*7*). Application of a neutralizing antibody for IFN-β confirmed autocrine/paracrine IFN-β–driven signaling in ADA2-depleted cells (Fig. 1F). Together, results establish ADA2 as an inhibitor of spontaneous IFN-β production.

Human endothelial cells express functional ADA2

We next sought to determine the mechanism by which ADA2 regulates innate immunity. Human ADA1 and ADA2 are isoenzymes that catalyze the irreversible deamination of adenosine (Ado) and deoxyadenosine (dAdo) to inosine (Ino) and deoxyinosine (dIno), respectively (*8*, *9*). *ADA2* mRNA transcripts are broadly expressed in human immune cells (fig. S2A) (*10*) and were detected in the monocytic cell line U937 and multiple primary human endothelial lineage cells by quantitative reverse transcription polymerase chain reaction (qRT-PCR) (Fig. 2A) and RNA sequencing (RNA-seq) in HUVEC (fig. S2B). A prior report failed to detect intracellular ADA2 protein or enzyme activity in HUVEC (*11*). However, ADA2 is an ectoenzyme having a classical signal peptide (*12*), and extracellular ADA2 protein was detectable in cultured supernatants of U937 and human endothelial cells by enzyme-linked immunosorbent assay (ELISA) (Fig. 2B) and Western blotting (Fig. 2C). In HUVEC, siADA2 reduced *ADA2* mRNA levels by ~75%, with no cross-reactivity against *ADA1* (fig. S2C). Similarly, siADA1 reduced *ADA1* mRNA levels by ~90%, with no cross-reactivity toward *ADA2* (fig. S2D). Analysis of deaminase activity, measured through de novo conversion of ^{15}N-labeled dAdo to dIno by mass spectrometry (MS), demonstrated that >90% of intracellular ADA activity measured in HUVEC whole-cell lysate was specifically reduced by ADA1 depletion and unaffected by ADA2 depletion (Fig. 2D). In contrast, extracellular ADA activity measured in HUVEC supernatant was reduced >75% by specific depletion of ADA2, with ADA1 accounting for a minority of extracellular activity (Fig. 2D), recapitulating results obtained in human plasma (*13*). To confirm ADA2-specific activity in HUVEC supernatants, dAdo to dIno conversion was measured in the presence of ADA2 siRNA and 50 μM erythro-9-(2-hydroxy-3-nonyl) adenine (EHNA) to selectively inhibit ADA1 activity (fig. S2E). Together, experiments demonstrate expression of functional ADA2 by HUVEC.

ADA2 and dAdo are paracrine modulators of IFNβ

To examine whether extracellular ADA2 activity is involved in IFN-β regulation, enzyme add-back experiments were performed in ADA2-depleted cells using recombinant ADA (rADA) proteins. Addition of rADA2 inhibited spontaneous induction of *IFN*-β, *CCL5*, and *CXCL10* mRNA in siADA2-treated HUVEC (Fig. 2E). Notably, rescue effects accompanied reconstitution of extracellular ADA activity to wild-type levels and were inhibited by pentostatin, a general inhibitor of ADA activity. Prior reports suggest that extracellular ADA2 may function independently of its nucleoside deaminase activity by exerting growth factor–like effects on cells (*8*, *12*). To confirm involvement of ADA activity in immune activation, rADA1 was added to ADA2-depleted cells, resulting in rescue of cytokine expression and extracellular ADA activity (Fig. 2E). Given the essential role of extracellular purine nucleoside deaminase activity in suppressing expression of innate cytokines, U937 cells were supplemented with exogenous nucleosides, and innate immune responses were examined. Supplementation of dAdo specifically induced IFN-β (Fig. 2F), suggesting that both ADA2 and dAdo act in a paracrine manner to modulate cellular innate responses. Accordingly, coculture of siADA2-treated HUVEC with untreated U937 cells provoked spontaneous IFN-β production in bystander U937 cells (Fig. 2G), confirming paracrine or non–cell autonomous effects of ADA2 in HUVEC.

Loss of ADA2 drives intracellular dAdo catabolism and accumulation of dIno

Extracellular Ado and dAdo are bioactive molecules that signal to immune cells during pathological inflammation (*14*, *15*). Ado and dAdo are released into the microenvironment in an autocrine/paracrine fashion or produced upon degradation of extracellular nucleic acids. Ado, but not dAdo, primarily signals via heterotrimeric GTP-binding protein (G protein)–coupled purinergic adenosine receptors (AdoR) (Fig. 3A), which elicit pleiotropic immune-modulatory effects. Alternatively, dAdo may be transported into cells via the action of nucleoside transporters. Vascular endothelial cells express relatively high levels of equilibrative nucleoside transporters (ENT) (Fig. 3B) that enable rapid and efficient clearance of dAdo from the blood (*16*) and may render these cells particularly sensitive to the effects of ADA2 deficiency and dysregulation of extracellular dAdo metabolism. Accordingly, incubation of HUVEC with ^{15}N-labeled dAdo resulted in rapid cellular uptake and equilibration of intracellular and extracellular dAdo pools within 5 min (Fig. 3C). Pretreatment with dipyridamole (DPM), a pharmacological inhibitor of ENT-mediated dAdo transport, reduced expression of the IFN-β and the IFN-β–driven gene signature in ADA2-depleted cells (Fig. 3D). Results indicate

Downloaded from http://advances.sciencemag.org/ on February 24, 2021

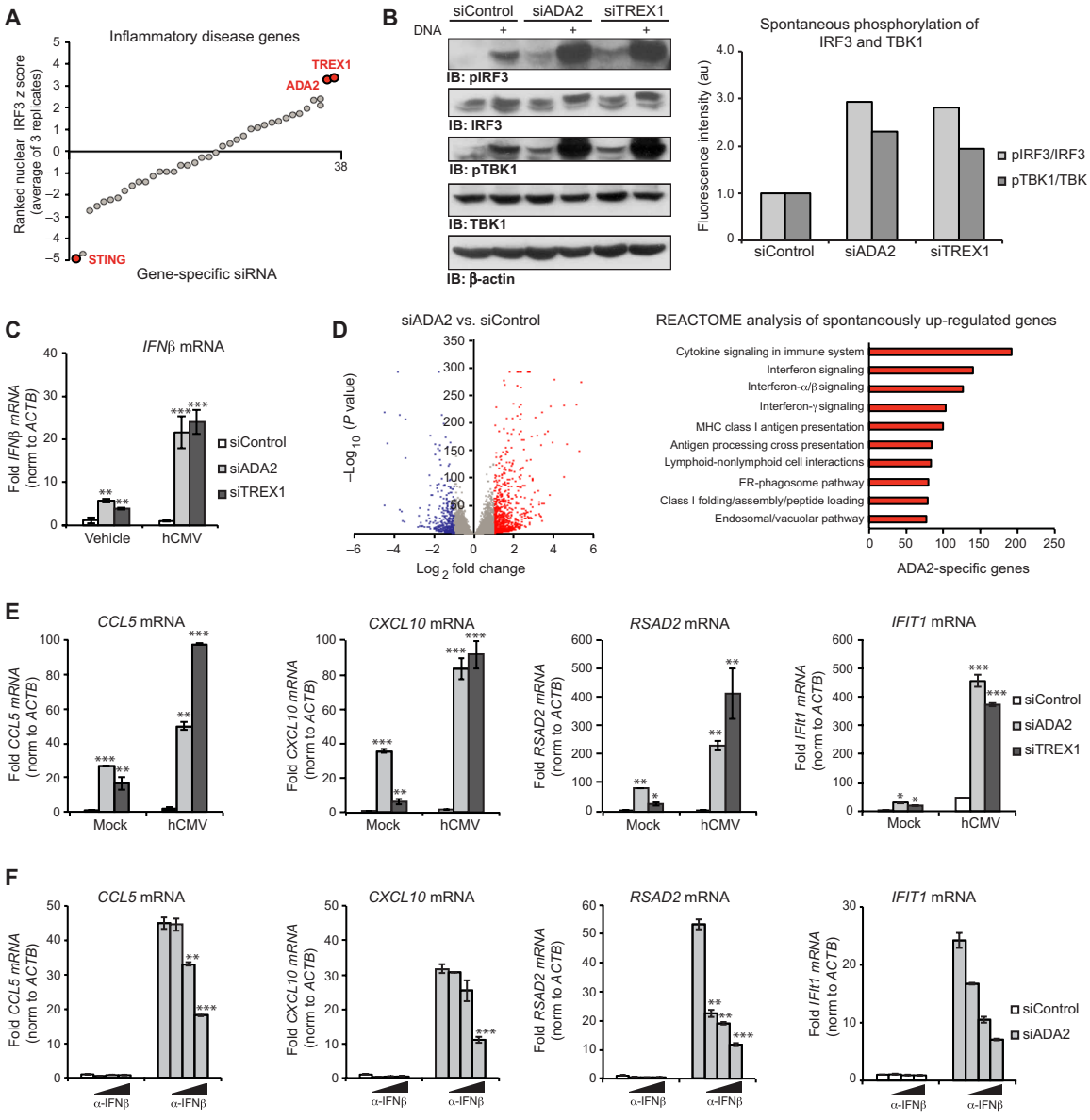

Fig. 1. Loss of ADA2 triggers spontaneous IFNβ production. (**A**) siRNA screen of 38 human disease genes in HUVEC (table S1), quantifying IRF3 nuclear translocation upon poly (dA:dT) DNA treatment (200 ng/ml for 3 hours). Averaged ranked *z* score for each gene-specific siRNA oligonucleotide pool is represented. STING, TREX1, and ADA2 scores are indicated in red ($n = 3$ technical replicates for $n = 3$ biological replicates, >200 single cells per technical replicate). (**B**) Western blot analysis of siControl, siADA2-, or siTREX-transfected HUVEC lysates (35 μg per lane). ImageJ quantification of the intensity ratio between phospho-IRF3/pan IRF3 and phospho-TBK1/TBK in unstimulated cells is shown in bar graphs. IB, immunoblot.; au, arbitrary units. (**C**) *IFN*-β mRNA levels, measured by qRT-PCR, in siControl, siADA2-, or siTREX1-transfected HUVEC upon treatment with vehicle or infection with hCMV [multiplicity of infection (MOI) = 1 for 3 hours] ($n = 3$ technical replicates). (**D**) Differential gene expression between siControl and siADA2-transfected HUVEC measured by polyadenylated poly (A^+)–enriched RNA-seq ($n = 3$ biological replicates) and REACTOME pathway analysis of the ADA2-specific genes. Red and blue dots denote genes significantly up- or down-regulated >2-fold. (**E**) Expression levels of IRF3-driven or IFN-β–driven genes, measured by qRT-PCR, in siControl, siADA2-, or siTREX1-transfected HUVEC upon mock or hCMV infection (MOI = 1 for 3 hours). (**F**) Expression levels of IRF3-driven or IFN-β–driven genes, measured by qRT-PCR, in siControl or siADA2-transfected HUVEC treated with IFN-β–neutralizing antibody (10, 20, and 40 U/ml) ($n = 3$ technical replicates). All results were replicated in three independent experiments. Values are presented as means ± SD. $^*P < 0.05$, $^{**}P < 0.01$, and $^{***}P < 0.001$. MHC, major histocompatibility complex; ER, endoplasmic reticulum; IB, immunoblot.

that cellular nucleoside transport of dAdo is essential for IFN-β production driven by reduced ADA2 enzyme activity.

Once taken up by cells, dAdo is metabolized through intracellular purine salvage and/or degradation pathways (Fig. 4A) (*15*), which may yield downstream effector molecules that influence innate signaling. To assess the potential intracellular fates of consumed extracellular dAdo, global MS-based metabolomics was performed (*17*). Comprehensive analysis of metabolites revealed intracellular accumulation of dIno and its downstream catabolite hypoxanthine in ADA2-depleted cells relative to control cells (Fig. 4, B and C), while

Downloaded from http://advances.sciencemag.org/ on February 24, 2021

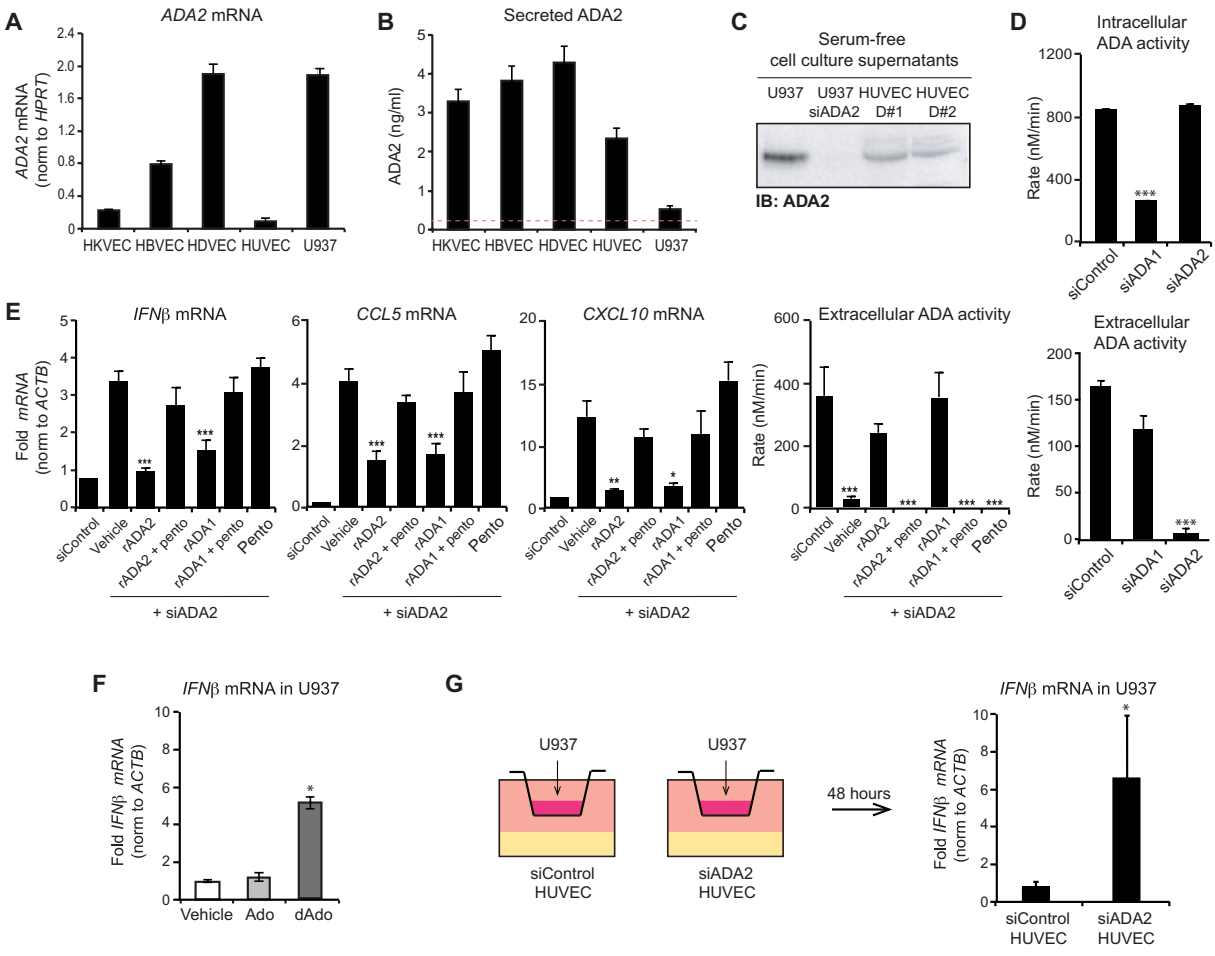

Fig. 2. Extracellular ADA2 and dAdo are paracrine modulators of IFNβ. (**A**) *ADA2* mRNA levels, measured by qRT-PCR, in primary endothelial cells and U937 monocytic cells ($n = 3$ technical replicates). (**B**) Secreted ADA2 protein, measured by ELISA, in primary endothelial cells and U937 monocytic cells ($n = 3$ technical replicates). (**C**) Secreted ADA2 protein, assessed by Western blotting of serum-free cell-conditioned supernatants, from HUVEC and U937 monocytic cells. (**D**) ADA activity, measured by de novo conversion of 1 mM isotopically labeled dAdo to dIno in whole-cell lysates (intracellular) or cell-conditioned supernatants (extracellular) from siControl, siADA1-, or siADA2-transfected HUVEC. Values are normalized to cell number and protein concentration ($n = 5$ technical replicates). (**E**) Expression levels of IRF3-driven or IFN-β–driven genes, measured by qRT-PCR, and extracellular ADA activity, measured by de novo conversion of 1 mM isotopically labeled dAdo to dIno in cell-conditioned supernatants, from siControl or siADA2-transfected HUVEC supplemented with rADA1 or rADA2 and pretreated with vehicle or pentostatin (10 μM for 30 min). Activity values are normalized to cell number and protein concentration ($n = 5$ technical replicates). (**F**) *IFN*-β mRNA, measured by qRT-PCR, in U937 monocytic cells supplemented with adenosine (Ado) or deoxyadenosine (dAdo) (100 μM for 48 hours) ($n = 3$ technical replicates). (**G**) *IFN*-β mRNA levels, measured by qRT-PCR, in U937 cocultured in Transwell inserts with siControl or siADA2-treated HUVEC for 48 hours ($n = 3$ technical replicates). All results were replicated in three independent experiments. Values are presented as means ± SD. $^{*}P \leq 0.05$, $^{**}P \leq 0.01$, and $^{***}P \leq 0.001$. HDVEC, dermal microvascular endothelial cells; HBVEC, brain microvascular endothelial cells; HKVEC, kidney microvascular endothelial cells.

other purine metabolites including dAdo and Ado were not changed (fig. S3A). These results show that loss of ADA2 activity dysregulates cellular purine catabolism and imply a compensatory mechanism by which extracellular dAdo is catabolized inside the cell. Consistent with this, addition of extracellular ^{15}N-labeled dAdo drove rapid intracellular accumulation of labeled dIno product in ADA2-depleted cells (Fig. 4C). Intracellularly, dIno is produced from consumed dAdo by ADA1 (Fig. 4A). Depletion of ADA1 in ADA2 knockdown cells suppressed both IFN-β expression and dIno production, demonstrating a functional role for ADA1 in producing intracellular dIno in the setting of ADA2 deficiency (Fig. 4D and fig. S3, B and C). In contrast, increasing intracellular dIno pools by silencing its catabolic enzyme PNP or silencing the cellular enzyme deoxycytidine kinase (dCK), an alternative enzyme for intracellular metabolism of dAdo (Fig. 4A), increased IFN-β levels (Fig. 4D and fig. S3C). Consistent with these observations, supplementation of exogenous dIno, but not Ino or hypoxanthine, was sufficient to trigger *IFN*-β mRNA production (Fig. 4E and fig. S3D), supporting a novel functional role for dIno in the cellular innate immune response. Notably, the immune-stimulatory effect of exogenous dIno was sensitive to DPM (fig. S3D) and was enhanced by pretreatment with 9-deazaguanine (Fig. 4E), which inhibits intracellular and extracellular catabolism of dIno by PNP. Data show that dIno accumulates intracellularly in ADA2-depleted cells due to the activity of ADA1 and functions as an immune-metabolite that is both necessary and sufficient for IFN-β induction.

Downloaded from http://advances.sciencemag.org/ on February 24, 2021

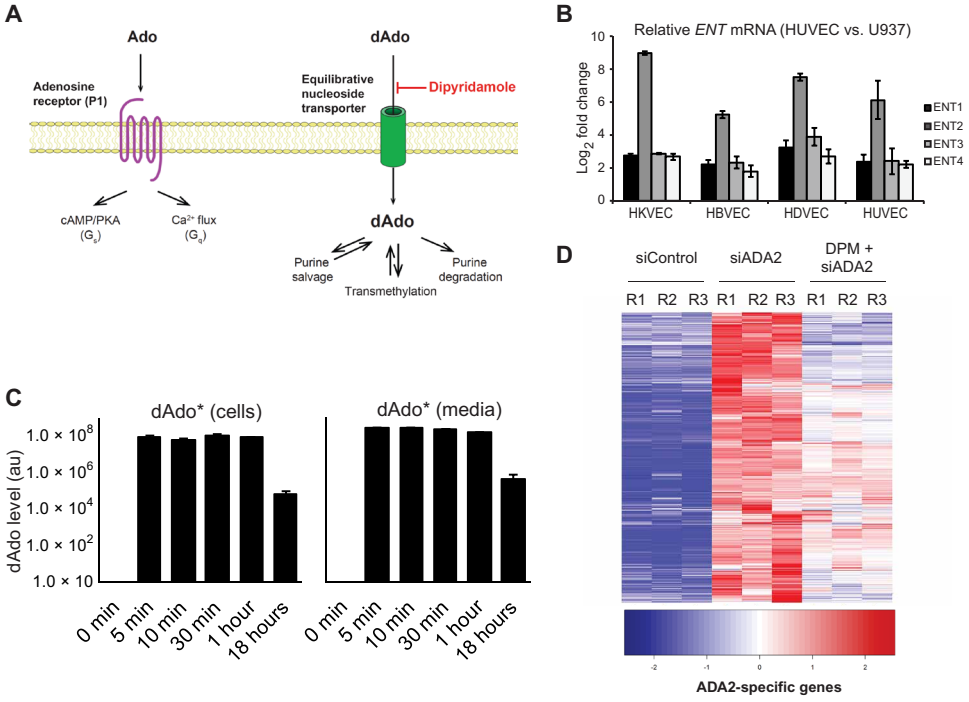

Fig. 3. Cellular nucleoside transport is required for induction of IFNβ upon depletion of ADA2. (**A**) Schematic representation of extracellular Ado receptor signaling and dAdo uptake/intracellular metabolism. cAMP, cyclic adenosine 3′,5′-monophosphate; PKA, cAMP-dependent protein kinase. (**B**) Equilibrative nucleoside transporter (*ENT*) mRNA levels, measured by qRT-PCR, in HUVEC and U937 ($n = 3$ technical replicates). (**C**) Extracellular and intracellular levels of isotope-labeled dAdo, measured by LC-MS/MS ($n = 5$ biological replicates). (**D**) Differential gene expression in siControl, siADA2-, or siADA2/DPM-treated (40 μM for 48 hours) HUVEC, measured by polyA$^+$ RNA-seq ($n = 3$ biological replicates). All results were replicated in three independent experiments. Values are presented as means ± SD. *$P \leq 0.05$.

dIno inhibits the cellular methionine cycle via SAM synthetase

We next sought to determine the mechanism by which dIno acts as an immunometabolite and functional regulator of innate immune signaling. Intracellularly, nucleosides and their analogs or metabolites interface with multiple cellular processes including transmethylation (*18*). Loss of ADA2 was associated with steady-state reduction in relative levels of L-cystathionine, a downstream metabolite in the methionine cycle, in siADA2-treated cells compared to controls (fig. S4A). To further examine methionine metabolism, time-course stable isotope tracing was performed with U-^{13}C methionine (*19*, *20*). Intracellular methionine metabolite pools were fully labeled within minutes of exposure to extracellular label, while *S*-adenosyl-methionine (SAM) and its downstream metabolite *S*-adenosylhomocysteine (SAH) acquired labeling over time (fig. S4B). The methionine M+4 mass isotopomer was consistently measured at ~2% (fig. S4C), suggesting a truncated cycle with little remethylation of homocysteine into methionine. Upon ADA2 depletion, SAM and SAH pools exhibited slower labeling over time relative to controls, and model-based metabolic flux analysis (*19*) revealed impaired cycle flux through the SAM synthetase [methionine adenosyltransferase (MAT)] and methyl-transferase (MT) reactions (Fig. 4F). In vitro enzyme activity assays demonstrated that dIno and, to a lesser extent, dAdo, but not the nucleoside cytidine, directly inhibited MAT activity (Fig. 4G). Accordingly, pharmacological inhibition of MAT using cycloleucine induced IFN-β (Fig. 4H), phenocopying the effects of ADA2 deficiency or dIno accumulation and suggesting a role for MAT inhibition in the immune-stimulatory effects of dIno. The MAT product SAM serves as a methyl donor for multiple enzymatic reactions, including DNA MT (DNMT)–dependent methylation of genomic cytosine bases (Fig. 4F). Accordingly, inhibition of DNMT using 5-azacytidine induced IFN-β (Fig. 4H). To examine the status of genomic transmethylation in ADA2-depleted cells, labeled methionine was used to monitor incorporation of methyl groups onto cytosine residues in genomic DNA. Control cells steadily accumulated labeled methyl-cytosine, reaching ~20 to 25% of genomic methyl-cytosine over 72 hours. In contrast, cells depleted of ADA2 or DNMT (Fig. 4I) and dIno-supplemented cells (fig. S4D) all demonstrated reduced de novo DNA methylation as early as 24 hours after the addition of label. These data demonstrate that dIno directly inhibits the activity of MAT and the methionine/SAM cycle, with subsequent reduction of genomic DNA transmethylation upon loss of ADA2 or supplementation with dIno.

Induction of methylation-sensitive endogenous retrovirus elements triggers IFNβ

Endogenous retrovirus elements (*ERV*) encode a diverse family of germline immune-stimulatory dsRNA-like molecules whose dynamic expression is particularly sensitive to genomic DNA hypomethylation. Overexpression of *ERV* in cells is directly linked to IFN-β production due to engagement of innate immune dsRNA sensing pathways (*21*, *22*). Loss-of-function studies confirmed that the cytosolic dsRNA sensors RIG-I and MDA5 and the dsRNA signaling adaptor MAVS drive spontaneous IFN-β production upon depletion of ADA2

Downloaded from http://advances.sciencemag.org/ on February 24, 2021

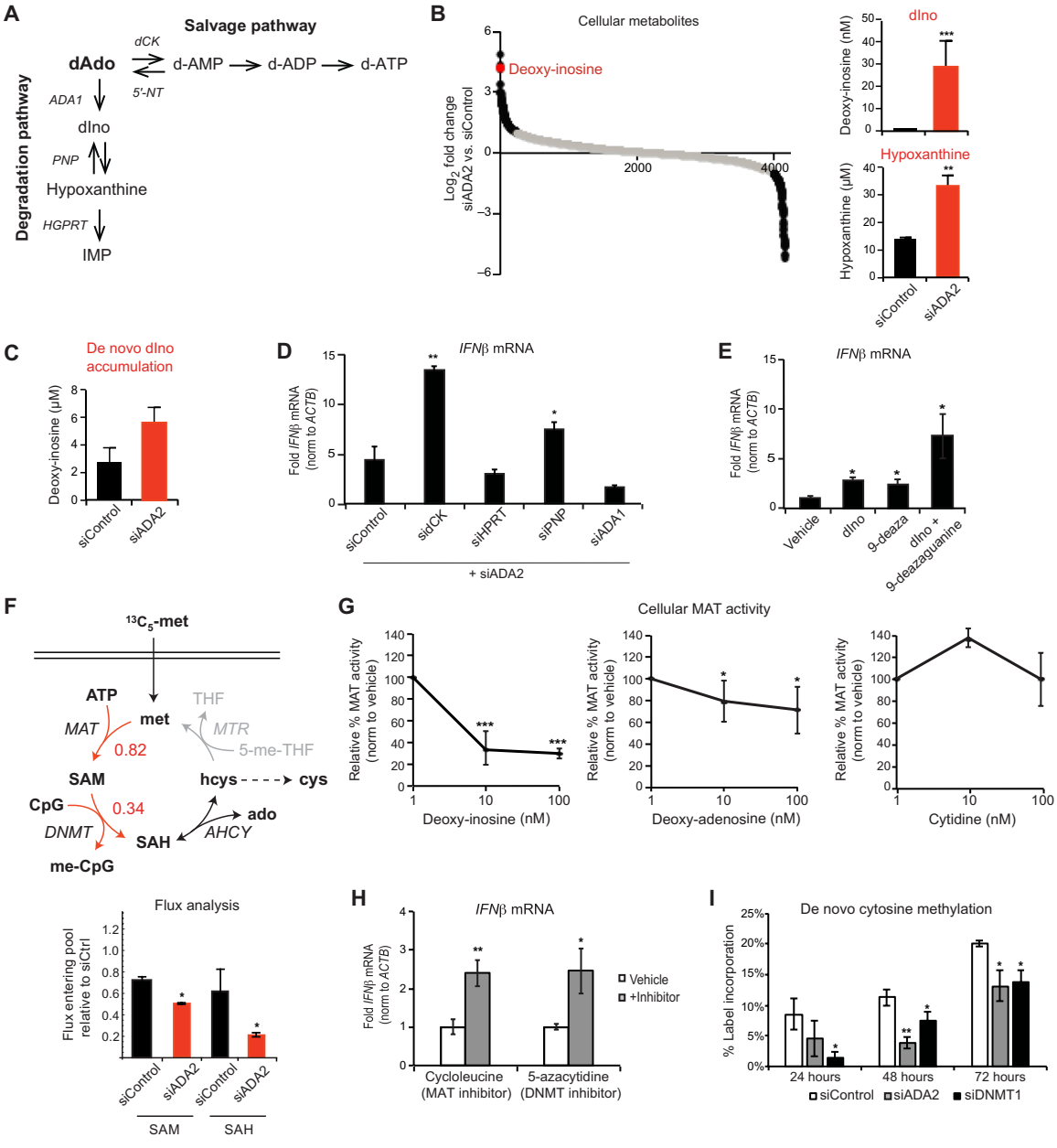

Fig. 4. Loss of ADA2 drives intracellular dAdo catabolism and accumulation of dIno. (**A**) Intracellular metabolic pathways of purine degradation [ADA1 (protein); PNP (protein); and HGPRT (protein), hypoxanthine phosphoribosyltransferase] and purine salvage [ADK (protein), adenosine kinase; dCK (protein), deoxycytidine kinase; and *5′-NT*, 5′-nucleotidase]. (**B**) Relative levels and concentrations of small-molecule polar metabolites measured by LC-MS/MS quantification of siControl or siADA2-transfected HUVEC ($n = 5$ biological replicates). (**C**) De novo accumulation of ^{15}N-dAdo–labeled dIno measured by LC-MS/MS quantification of siControl or siADA2-treated HUVEC ($n = 5$ biological replicates). (**D**) *IFN*-β mRNA levels, measured by qRT-PCR, in HUVEC transfected with siRNAs targeting ADA2 and ADA1, PNP, HGPRT (protein), or dCK. (**D**) *IFN*-β mRNA levels, measured by qRT-PCR, in HUVEC supplemented with dIno (500 μM for 24 hours) or (**E**) pretreated with the PNP inhibitor 9-deazaguanine (100 μM for 30 min) before dIno supplementation (500 μM for 24 hours) ($n = 3$ technical replicates). (**F**) Flux analysis of the methionine/SAM cycle, measured by LC-MS/MS quantification of U-^{13}C methionine–labeled methionine, SAM, and SAH, in siControl or siADA2-treated HUVEC ($n = 5$ biological replicates). (**G**) Methionine adenosyltransferase (MAT) enzyme activity, measured by LC-MS/MS quantification of SAM, in HUVEC lysates supplemented with nucleosides ($n = 3$ technical replicates). (**H**) *IFN*-β mRNA levels, measured by qRT-PCR, in HUVEC pretreated with cycloleucine (MAT inhibitor, 20 mM for 30 min) or 5-azacytidine (DNMT inhibitor, 500 nM for 30 min) ($n = 3$ technical replicates). (**I**) De novo DNA methylation, measured by LC-MS/MS quantification of U-^{13}C-methionine labeled 2′-deoxy-5-methylcytidine in siControl, siADA2-, or siDNMT1-treated HUVEC ($n = 3$ biological replicates). Values are represented as the percentage of total label incorporation. All results were replicated in three independent experiments. Values are presented as means ± SD. *$P \leq 0.05$, **$P \leq 0.01$, and ***$P \leq 0.001$. ADP, adenosine diphosphate; IMP, inosine monophosphate; THF, tetrahydrofolate; MTR, 5-methyltetrahydrofolate-homocysteine methyltransferase or methionine synthase.

Downloaded from http://advances.sciencemag.org/ on February 24, 2021

(Fig. 5A and fig. S5A). Analysis of transcriptomic data obtained in ADA2-depleted cells to specifically examine expression of long terminal repeat (LTR)–containing genomic sequences, which comprise a large portion *ERV* elements, revealed overexpression of >30 LTR-containing *ERV*-like molecules (Fig. 5B). Furthermore, *ERVFRD-1* and *ERVK28* genes were highly induced after supplementation with dIno or depletion of ADA2 (Fig. 5, C and D). Augmented expression of *ERV* in dIno-treated cells (24 hours; Fig. 5C) or ADA2-depleted cells (24 to 48 hours; Fig. 5D) was detectable prior to induction of *IFN*-β mRNA (72 hours; fig. S5B) and occurred independently of autocrine/paracrine IFN-β–driven signaling (Fig. 5E and fig. S5F). To confirm the immune-stimulatory effects of *ERV*, transcript variants of *ERVK28* were overexpressed in HUVEC, resulting in spontaneous induction of *IFN*-β, *CCL5*, and *CXCL10* (Fig. 5F). Results demonstrate that overexpression of immune-stimulatory *ERV* in ADA2-depleted cells drives the IFN-β response.

DISCUSSION

Here, we report a new cellular strategy for triggering IFN-β production by extracellular dAdo (Fig. 6). Loss of the ectoenzyme ADA2 or direct supplementation of exogenous dAdo drives cellular transport and catabolism by the cytosolic enzyme ADA1, driving de novo dIno production and dIno accumulation inside ADA2-depleted cells. dIno is a functional immune-metabolite that directly inhibits the cellular methionine cycle at the level of MAT, thereby suppressing cellular transmethylation reactions. Genomic hypomethylation provokes overexpression of immune-stimulatory *ERV* transcripts, including *ERVK28* and *ERVFRD-1*, which trigger IRF3 activation and IFN-β. Thus, purine nucleoside metabolism by ADA2 and other enzymes involved in extracellular DNA metabolism is likely an important determinant of IFN-β and IFN-β–driven gene expression in inflammatory microenvironments, where inappropriate release and accumulation of cell-free DNA and its nucleoside

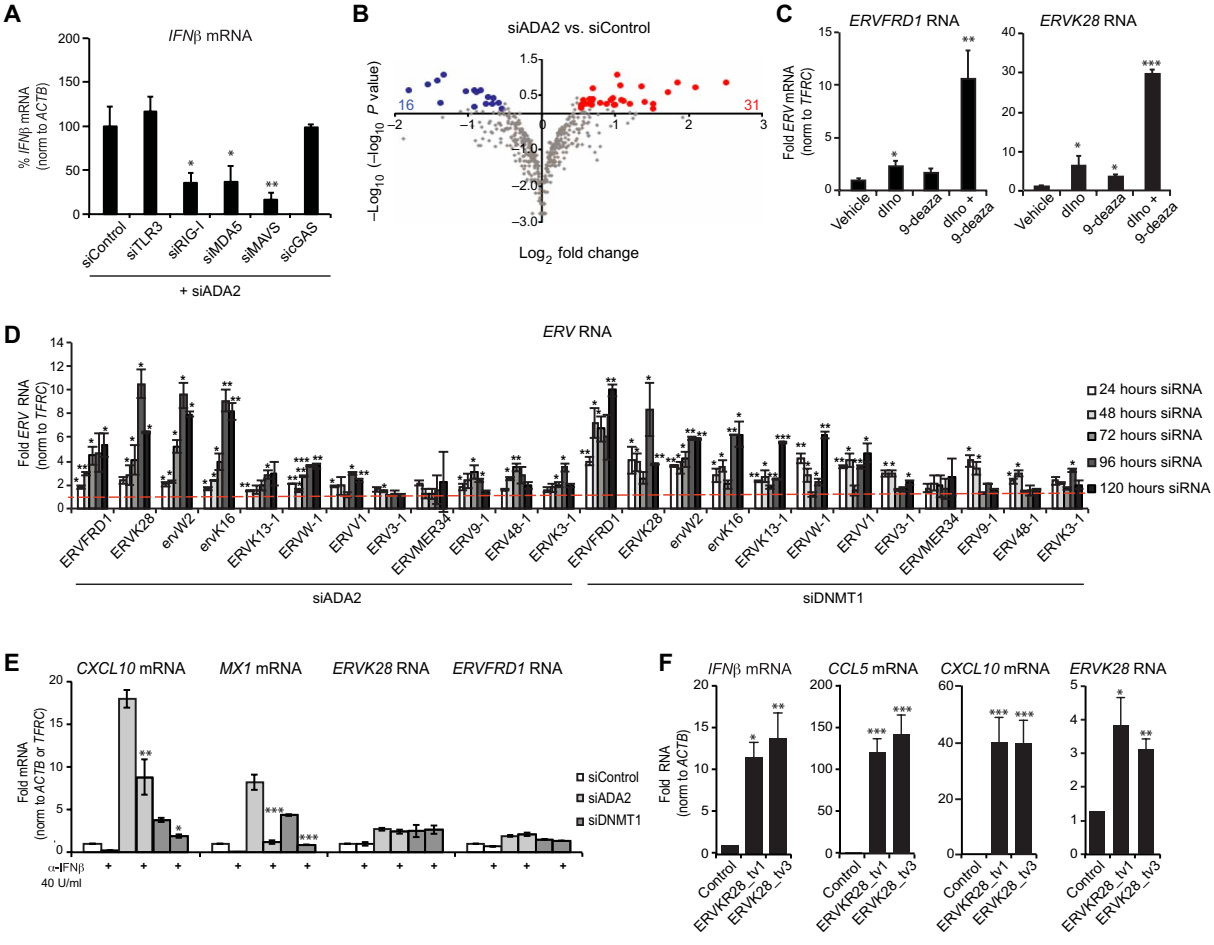

Fig. 5. Induction of methylation-sensitive ERV triggers cytosolic dsRNA signaling and IFNβ production. (**A**) *IFN*-β mRNA levels, measured by qRT-PCR, in HUVEC transfected with siRNAs targeting ADA2 and innate sensing molecules ($n = 3$ technical replicates). (**B**) Differential expression of LTR-containing *ERV* genes between siControl and siADA2-transfected HUVEC, measured by polydenylated poly(A^+)–enriched RNA-seq ($n = 3$ biological replicates). Red and blue dots denote *ERV* significantly up- or down-regulated ≥1.5-fold. (**C**) mRNA levels of *ERVFRD1* and *ERVK28*, measured by qRT-PCR, in HUVEC supplemented for 24 hours with dIno (500 μM) or pretreated for 30 min with the PNP inhibitor 9-deazaguanine (100 μM) before dIno supplementation for 24 hours ($n = 3$ technical replicates). (**D**) mRNA levels of *ERV* at 24 to 120 hours, measured by qRT-PCR, in siADA2- or siDNMT1-transfected HUVEC ($n = 3$ technical replicates). (**E**) mRNA levels of *ISG* and *ERV*, measured by qRT-PCR, in siADA2-transfected HUVEC treated with anti–IFN-β–neutralizing antibody (40 U/ml) ($n = 3$ technical replicates). (**F**) *ERV*, *IFN*-β, *CCL5*, and *CXCL10* mRNA levels, measured by qRT-PCR, in HUVEC transfected with control plasmid or plasmids encoding *ERVK28* transcript variants. Values are presented as means ± SD. $^*P \le 0.05$, $^{**}P \le 0.01$,a nd $^{***}P \le 0.001$.

Downloaded from http://advances.sciencemag.org/ on February 24, 2021

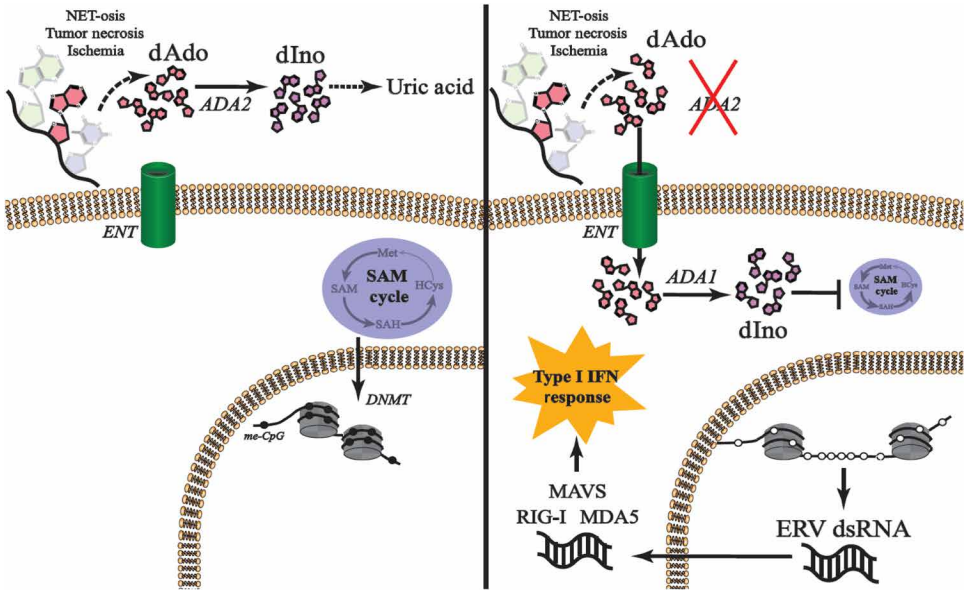

Fig. 6. Cellular sensing of extracellular purine nucleosides triggers an innate immune response. Loss of extracellular ADA2 activity or an excess of extracellular purine nucleosides drives uptake of dAdo and intracellular catabolism by ADA1, yielding dIno, an immune-metabolite that directly inhibits MAT activity, the methionine cycle, and DNA methylation. Genomic hypomethylation drives up-regulation of *ERV*, dsRNA molecules that engage cytosolic dsRNA sensors RIG-I and MDA5 via the signaling adaptor MAVS.

by-products accompanies infection, ischemic injury, and tumor growth.

The ADA2/ADA1 axis controls bioactivity of purine nucleoside metabolites

Results presented here show that cellular innate immunity is triggered by a unique immune-metabolic axis that balances competing, compartmentalized ADA activities in the extracellular and cytosolic spaces. Differential effects of ADA2 and ADA1 depletion on IFN-β expression in HUVEC underscore the complex nature of bioactive purines in modulating immune cells and inflammation. In the extracellular space, Ado exerts pleiotropic effects on innate and adaptive immune cells from signals generated via purinergic G protein–coupled receptors or ligand-gated ion channels (*14*). Because of the broad expression of the A2A and A2B adenosine receptor isoforms (AdoR) in the immune compartment, extracellular Ado exerts substantial anti-inflammatory effects on cells. Here, we show that extracellular dAdo exerts a proinflammatory effect due to triggering of cellular IRF3 activation, IFN-β production, and an IFN-β–driven innate immune response that up-regulates an array of proinflammatory cytokines, chemokines, and signaling proteins (Fig. 1D). Ultimately, the magnitude, duration, and outcome of competing immune-suppressive and immune-stimulatory purine signals at a given immunological niche will depend on metabolic activities of cellular purine salvage or degradation enzymes, as well as ectonucleases and ectonucleotidases such as deoxyribonuclease I (DNAse I), CD39, and CD73 that catalyze Ado and dAdo production from cell-free RNA or DNA in circulation. These enzymes are the key targets for modulating the purine pathway and thus developing novel strategies for immunotherapy.

In HUVEC, ADA activities are compartmentalized such that ADA2 accounts for >75% of extracellular activity, and ADA1 accounts for all intracellular activity (Fig. 2D). Extracellular activity in HUVEC-conditioned supernatants accurately reflects human plasma, where total circulating ADA activity measured in healthy individuals specifically correlates with the ADA2-specific activity (*13*, *23*). Median ADA1 activity measured in normal human plasma accounts for ~25% (*13*), recapitulating results obtained here using gene-specific siRNAs. Despite data from multiple studies demonstrating that ADA2 accounts for most of extracellular ADA activity measured in human plasma, it has nonetheless been postulated that ADA2 plays a minimal role regulating purine metabolism in vivo. This is variously attributed to the particular biochemical properties of ADA2, putative growth factor–like properties of ADA2, and lack of Ado/dAdo elevation in ADA2 deficiency disease (DADA2) patient plasma. Data obtained using rADA2 and rADA1 proteins (Fig. 2E) or dAdo supplementation (Fig. 2F) unequivocally demonstrate that ADA enzymatic activity regulates IFNβ expression. Regarding the biochemistry of ADA2, many early studies reporting enzyme reaction rate and substrate affinity were obtained using purified protein preparations that are highly unstable (*9*) and may have underestimated the actual enzyme activity in vivo. Furthermore, ADA2 activity assays in plasma and cell-conditioned supernatants typically use relatively high nucleoside concentrations (e.g., 1 mM); however, our results were fully recapitulated at a range of dAdo concentrations as low as 100 nM. Notably, ADA2 exhibits a broadly optimal pH range compared to ADA1 (*8*, *9*), suggesting that it may be specifically suited to pathological conditions when release of lactic acid or reduced blood flow/hypoxia drives pH down, which substantially impairs normal metabolic activities and potentially impairs ADA1. Circulating ADA2 activity is specifically increased upon HIV infection (*24*), chronic hepatitis (*25*), rheumatoid arthritis (*26*), and tuberculosis (*27*) and has repeatedly been proposed as a diagnostic tool or surrogate biomarker for multiple human inflammatory diseases. Our new mechanistic insights regarding cellular innate immunity provide a key missing component in our understanding of ADA2 as

Downloaded from http://advances.sciencemag.org/ on February 24, 2021

a functional regulator of immunity and inflammation rather than a passive biomarker.

While ADA2 has a signal peptide that directs trafficking through classical protein secretion pathways, ADA2 intracellular protein stores appear to be selectively retained in the cytoplasm of myeloid cells and mobilized upon cellular stimulation. In contrast to endothelial cells in which intracellular ADA2 protein (*11*) and enzyme activity (Fig. 2D) is undetectable, monocytes and macrophages retain ADA2 inside cells (*11*). Upon cellular stimulation with phorbol esters and calcium ionophore, intracellular stores of ADA2 are acutely mobilized into the extracellular space (*28*), likely contributing to increased ADA2 activity observed in vivo in human plasma. Transcriptional profiles obtained from unbiased analysis of human hematopoietic cell subsets (*10*) revealed broad expression of ADA2 mRNA in many immune cell types (fig. S2A), where regulated retention and release of ADA2 might be at play during the course of physiological inflammation in vivo. Elucidating the specific signals that regulate inducible ADA2 activity during inflammation will require developing an appropriate, multicellular immunocompetent system, in which ADA1 and ADA2 expression and compartmentalization are conserved.

Extrinsic sensing of DNA danger signals

Like ADA2, extracellular accumulation of bioactive nucleosides also occurs during inflammation upon acute damage to cells and tissues (*14*). Driving local concentrations of extracellular nucleotides and nucleosides well above their homeostatic levels in circulation could exceed the catabolic capacity of ADA2 enzyme activity, pushing cellular equilibrium in favor of nucleoside uptake by the vascular endothelium and other cells. Both Ado and dAdo typically display a half-life of seconds in circulation due to rapid and efficient uptake by vascular endothelial cells (*16*), which express relatively high levels of nucleoside transporters (Fig. 3B) and may confer particular sensitivity to the functional effects of ADA2 deficiency and extracellular dAdo.

Acute elevations of extracellular adenosine triphosphate (ATP) and Ado up to micromolar concentrations have been quantified in vivo upon ischemia in the brain (*29*) and heart (*30*). Extracellular accumulation of dAdo is less well documented; however, a recent unbiased metabolic characterization of myocardial infarction in humans showed that sustained plasma elevations of dAdo occurred during the reperfusion phase of ischemic tissue (*31*), when the bulk of vascular injury and inflammation occurs. Ischemia/reperfusion injury provokes a robust innate type I IFN response (*32*), which is likely to be affected by the dAdo-dependent mechanism reported here. In the solid tumor microenvironment, chronic elevation of Ado at micromolar concentrations plays a critical role in modulating tumor-infiltrating immune cells (*33*). Notably, induction of ERV in tumors drives a protective antitumor IFN-β response (*21*) and is associated with increased survival (*22*), suggesting that enhanced dAdo uptake may play a protective role in the tumor microenvironment by boosting tumor immune surveillance.

Cell-free DNA also accumulates in circulation during pathological inflammation (*4*), and dAdo may be produced upon breakdown of extracellular DNA by circulating DNAse I (*34*). This is particularly relevant for infections and other pathological processes that stimulate the formation of neutrophil extracellular traps (NETs), a unique form of cell death in which decondensed chromatin is released into the extracellular environment by activated neutrophils. A recent study reported enhanced NETosis in cells from DADA2 patients, which was linked to increased Ado signaling via adenosine receptors expressed on neutrophils (*35*). Thus, it is likely that increased NETosis, subsequent release of cellular DNA coupled, and dysregulated dAdo metabolism in ADA2 patients could synergize to drive innate cytokine responses in DADA2 patients. This is of relevance for microbial infections in which excessive neutrophil activation drives pathogenic inflammation, such as the novel coronavirus disease 2019 (COVID-19), which drives excessive NETosis and cytokine-driven pathogenic inflammation in the human lung (*36*).

Clarifying the cellular and molecular mechanisms governing extracellular DNA-DAMP signaling will be necessary to understand how protective or pathogenic inflammatory signals are initiated, propagated, and amplified during the course of inflammatory episodes. In this regard, specialized myeloid cells can sense and respond to immune-stimulatory DNA triggers using both cell-intrinsic and cell-extrinsic mechanisms. This signaling diversity enables these specialized cells to report intrinsic inflammatory provocations or amplify extrinsic signals. Accordingly, here, we show that monocytic cells respond to paracrine effects of ADA2 and dAdo by triggering IFN-β. Whether nonphagocytic or stromal cells can sense external DNA-DAMP triggers, allowing them to amplify inflammation in response to external innate ligands, is unclear. Our results in HUVEC establish purine nucleosides as broadly acting immune-stimulatory agents of sterile inflammation and implicate cellular sensing of extracellular purines as a unique modality, enabling non-specialized cells to fulfill a specialized innate immune function by responding to DNA-DAMP signals originating from distal cell damage. This is relevant to the as-yet incomplete understanding of the origins of innate inflammatory signals in human autoimmune disease and vasculitis, and our data suggest that stromal cells of the vascular endothelium are initiators of inflammatory signals rather than bystanders.

ADA2 deficiency disease

Our previously unknown results linking reduced ADA2 ectoenzyme activity and dysregulated purine nucleoside signaling to spontaneous IFN-β production expands our understanding of the complex and seemingly conflicting pathobiology of DADA2, a poorly understood immunological disease affecting several hundred patients worldwide, primarily children. Many patients with DADA2, whose clinical diagnosis is contingent upon specific reduction of serum ADA2 enzyme activity or loss-of-function mutations in the *ADA2* gene (*11*, *37*), experience clinical symptoms ranging from multiorgan vascular inflammation of the brain, skin, and kidneys to primary immunodeficiency due to bone marrow failure. Our data show that ADA2 deficiency exerts paracrine effects on the immune response that directly relate to dysregulated dAdo/dIno metabolism. Notably, extracellular accumulation of dAdo neither was observed in ADA2-deficient HUVEC nor was it required for spontaneous IFN-β induction (Fig. 3B). Rather, ENT- and ADA1-dependent production of dIno, dysregulation of genomic DNA methylation, and *ERV* induction drove cellular IFN-β production. DADA2 patients do not exhibit steady-state elevations of dAdo in the blood (*11*); however, intracellular measurements of purine metabolites and *ERV* have not been reported in myeloid and stromal cells from these individuals. Furthermore, since steady-state levels of dAdo measured in systemic circulation do not necessarily reflect localized

Downloaded from http://advances.sciencemag.org/ on February 24, 2021

or dynamic changes in dAdo levels in inflamed tissues or organs, development of an appropriate in vivo or multicellular system will be required to accurately assess effects of ADA2 deficiency on dynamic changes in dAdo levels.

Notable similarities exist between DADA2 and other metabolic syndromes of purines in humans; approximately one-third of patients harboring loss-of-function mutations in PNP, the enzyme that catabolizes dIno, present with elevated levels of dIno and autoimmune manifestations (*38*). These include systemic lupus erythematosus (SLE), a disease of multiorgan autoinflammation and vasculitis, in which elevated type I IFN production is causally implicated. Recently, an unbiased genetic analysis of human SLE identified missense single-nucleotide polymorphisms in the coding region of the *PNP* locus, which correlated in a dose-dependent manner to low PNP expression, low PNP enzyme activity, and high circulating levels of IFN (*39*). The mechanism of IFN up-regulation is unknown but may interface with the novel mechanism described here. The overlapping immunological manifestations of DADA2 and PNP deficiency disease, which run the spectrum of immune deficiency to autoimmunity, support overlapping immune-modulatory mechanisms involving purine nucleosides.

The functional significance of IFN-β in the pathobiology of DADA2 or PNP deficiency disease is not well understood. Notably, IFN-β–driven signaling promotes immune cell activation and drives additional inflammatory cytokines, including tumor necrosis factor (TNF). Notably, elevated TNF is not detectable in the serum in DADA2 patients; however, its functional relevance in driving vascular inflammation in DADA2 arises from the clinical observation that inhibitors of TNF effectively control symptoms of inflammatory vasculopathy and prevent strokes (*40*). Both IFN-β and TNF are functional drivers of pathology in SLE (*41*). In macrophages, TNF induces low levels of IFN-β, and autocrine TNF signaling synergizes with autocrine IFN-β signaling to enhance the expression of proinflammatory genes. Notably, neither control nor ADA2-depleted HUVEC expresses detectable levels of TNF, either at baseline or in response to innate ligands and virus infection. However, our data support a paracrine effect for IFN-β produced by vascular endothelium in driving TNF expression in macrophages. Imbalanced macrophage polarization toward the proinflammatory M1 macrophage phenotype is characteristic of DADA2 disease (*11*), and M1 macrophages are a primary source of TNF in vivo. IFN-β–driven signaling actually drives M1 polarization through activation of the transcription factor signal transducers and activators of transcription 1 and up-regulation of M1-promoting cytokines CXCL10 and CXCL9 (*42*). Thus, our data support a model whereby spontaneous IFN-β produced by vascular endothelium can drive down TNF production by M1 macrophages.

A primary limitation of our study is an absence of in vivo corroboration that ADA2 deficiency or extracellular purine nucleosides drive IFN-β production in stromal and immune cells. This is compounded by the lack of conservation of ADA2 in the mouse and the heterogenous nature of DADA2 disease, which likely affects many different cell types due to autocrine/paracrine activities of ADA2 and purine nucleosides and the variable nature of extracellular purine accumulation. Future studies centered on studying other regulatory enzymes of purine nucleoside metabolism using mouse models of tumor growth, infection, or ischemia, as well as studies of both stromal and immune cells isolated from DADA2 patients undergoing acute manifestations of inflammatory disease, will be required to further understand the complex balance between the proinflammatory and anti-inflammatory activities of purine nucleosides in human disease.

MATERIALS AND METHODS

Experimental design

The objective of this research is to examine novel molecular mechanisms regulating the innate immune IFN-β response using controlled laboratory experiments. To identify novel gene and protein regulators of IFN-β, we optimized and implemented loss-of-function RNA interference screening for activation of the transcription factor IRF3 in primary human vascular endothelial cells. Among 38 candidates associated with systemic inflammation and vasculitis in humans, the metabolic enzyme ADA2 was identified as a novel negative regulator of spontaneous IFN-β production. Subsequent transcriptomic, metabolic, and functional experiments were performed to examine the effects of ADA2 deficiency and purine nucleoside supplementation in triggering IFN-β via activation of cytosolic nucleic acid sensing pathways.

Study design

Sample size (*n*) for each experimental group is described in each figure legend and was determined on the basis of the optimal number to generate statistically significant data. No data were excluded. All experimental findings were independently replicated three times. Outliers were identified at the beginning of the study. Samples were randomized by position on plates, microplates, and flow cells or temporally randomized on the mass spectrometer. For siRNA screening, qRT-PCR, RNA-seq, and MS, research subjects (e.g., cell culture supernatants or lysates) were analyzed in a blinded manner using numerical keys.

Antibodies and reagents

rADA1 (93985) was purchased from Sigma-Aldrich, and rADA2 (7518-AD) was from R&D Systems. ADA2 antibody (HPA007888) was purchased from Sigma-Aldrich, and β-actin antibody (MAB8929) was from R&D. Toll-like receptor 3 antibody (sc-32232) was from Santa Cruz Biotechnology, cGAS antibody (AP10510c) was from Abgent, and DDX58/RIG-I (ab45428), MAVS (ab31334), and IFI16 (ab55328) antibodies were from Abcam. IFIH1/MDA5 antibody (21775-1-AP) was purchased from Proteintech, and phospho-IRF3 (Ser^{396}) (4947S), phospho-TBK1 (Ser^{172}) (5483S), TBK1 (3013S), and IRF3 (4302S) antibodies were from Cell Signaling Technologies. Human IFN-β–neutralizing antibody (31401-1) was purchased from PBL IFN source, and 2′-deoxyadenosine, adenosine, DPM, EHNA, 5-azacytidine, and 9-deazaguanine were from Sigma. Pentostatin was purchased from Cayman Chemicals, cycloleucine was from MP Biomedicals, and 2′-deoxyinosine, inosine, and hypoxanthine were from Alfa Aeser. ELISA kit for ADA2 quantification in cell culture supernatants was purchased from Cloud Clone Corp. poly (dA:dT) DNA was purchased from Invivogen. poly (dA:dT) DNA (P0883) was purchased from Sigma.

Cells

Primary human cells were obtained from Lonza as single-donor aliquots. HUVEC and aortic endothelial cells were maintained in EGM-2 BulletKit growth media (Lonza) supplemented with 2%

Downloaded from http://advances.sciencemag.org/ on February 24, 2021

hi-FBS (fetal bovine serum). Dermal microvascular endothelial cells, brain microvascular endothelial cells, and kidney microvascular endothelial cells were maintained in EBM-2MV BulletKit growth media (Lonza) supplemented with hi-FBS. Normal bronchial epithelial cells were maintained in BEGM BulletKit growth media (Lonza). U937 monocytes were obtained from American Type Culture Collection and maintained in RPMI supplemented with hi-FBS. Purity of cell populations was verified >95% by flow cytometry using the following markers: CD31 for endothelial cells (BioLegend, 303121), epithelial cell adhesion molecule for epithelial cells (BioLegend, 324207), and CD45 for U937 monocytes (BioLegend, 103115). For activation of IRF3-driven responses, cells were transfected with poly dA:dT for 3 hours (200 ng/ml) using LyoVec transfection reagent (Invivogen) or infected for 3 hours with hCMV strain MOLD [multiplicity of infection (MOI) = 1]. For IFN-β neutralizing experiments, cells were treated with anti–IFN-β–neutralizing antibody (10 to 40 U/ml) for 72 hours.

Virus

hCMV clinical strain MOLD (a gift from M. Raftery) was used. Stocks were prepared as previously described (*6*).

siRNA screening and transfections

siGenome siRNA oligonucleotide pools were purchased from Dharmacon, and transfections were performed as previously described (*6*). siRNA transfection in U937 was performed with a Neon Transfection System 100 μl kit (Thermo Fisher Scientific). Cells were resuspended with R buffer (5×10^6 cells/ml) and electroporated with 100 nM siRNA at 1400 V/10 ms/3 pulse. Following transfection with siRNA (30 to 40 nM), growth media was changed every 24 hours, and cells were harvested after 72 hours unless otherwise specified. For the IRF3 screen, *z* score was calculated for each gene-specific siRNA pool using mean and SD values from triplicate wells compared to control, nontargeting siRNA (Dharmacon). Individual *z* scores are listed in table S1. siRNA sequences are listed in table S2.

IRF3 immunostaining

IRF3 immunostaining was performed as described (*6*). IRF3 antibody (sc-9082) was purchased from Santa Cruz Biotechnology, and Alexa Fluor 647–conjugated anti-rabbit secondary antibody (111-604-144) was from Jackson ImmunoResearch. DAPI (4′,6-diamidino-2-phenylindole) was used to counter stain nuclei. Images were acquired at ×10 magnification on ImageXpress Micro (Molecular Devices), and images were analyzed using the enhanced translocation module of MetaXpress (Molecular Devices). Individual cells were scored as positive for nuclear translocation if >70% of IRF3 fluorescence were spatially correlated with nuclear probe. Each data point is representative of >200 cells.

Quantitative real-time PCR

Total RNA was extracted using a Quick-RNA MiniPrep Plus kit (Zymo Research). RNA (500 ng) was used to synthesize complementary DNA (cDNA) using a qScript cDNA synthesis kit (Quanta). Samples were diluted 10-fold, and gene expression was analyzed on a CFX96 Touch Detection System (Bio-Rad) using FastStart SYBR Green Master Mix (Roche) or TaqMan Universal PCR Master Mix (Thermo Fisher Scientific). Primer pair sequences and catalog numbers for cellular mRNAs are listed in table S3. Primer pair and catalog numbers for ERV genes are listed in table S4.

Western blotting

For Western blotting of whole-cell lysates, cells were lysed in 1X radioimmunoprecipitation assay buffer (Cell Signaling Technology), incubated on ice for 30 min, and centrifuged at 10,000 rpm for 10 min. Protein concentration was quantified from cleared supernatants using bicinchoninic acid protein assay kit (Thermo Fisher Scientific). Equivalent amounts of lysate (30 to 50 μg) were boiled with 5× SDS sample buffer and resolved by 10% SDS–polyacrylamide gel electrophoresis (SDS-PAGE), transferred to polyvinylidene difluoride membrane (Thermo Fisher Scientific), blocked with 5% milk, and incubated with primary antibody (1:1000) at 4°C overnight. Blots were washed with tris buffered saline-0.1% tween 20 and incubated with horseradish peroxidase–conjugated secondary antibodies (1:7000) at room temperature for 1 hour. Signal was detected using Amersham ECL Prime (GE Healthcare). For Western blotting of cultured supernatants to detect ADA2, HUVEC or U937 cells plated at 5×10^5 cells per well in six-well plates in serum-free media were cultured for 48 hours before collecting supernatants. Supernatant (2 to 6 ml) was filtered (0.45-μm filter, 28413-312, VWR) and concentrated with Pierce Protein Concentrator polyethersulfone 10K molecular weight cutoff (88527, Thermo Fisher Scientific) at 5000 rpm for 15 min to obtain 100 to 150 μl of samples. Concentrated supernatants were incubated with 5x SDS sample buffer at 70°C for 10 min and resolved by 10% SDS-PAGE as described above. ADA2 antibody was obtained from Sigma (HPA007888).

RNA sequencing

Total RNA was extracted from 2×10^5 cultured cells using the Quick-RNA MiniPrep samples and samples were checked for RNA integrity number equivalent (RIN^e) scores above 9.0. For each sample, 500 to 1000 ng of total RNA were then prepared into an mRNA library using the TruSeq Stranded mRNA Library Prep Kit (Illumina). Resulting libraries were then pooled at equimolar concentrations using the Quant-iT PicoGreen double-stranded DNA Assay Kit (Life Technologies) and were deep sequenced on an Illumina 2500 in Rapid Run Mode, producing between 10 and 90 M single-end reads with lengths of 50 nucleotides per sample. The single-end reads that passed Illumina filters were filtered for reads aligning to transfer RNA (tRNA), ribosomal RNA (rRNA), adapter sequences, and spike-in controls. The reads were then aligned to University of California, Santa Cruz hg38 reference genome using TopHat (v1.4.1). DUST scores were calculated with PRINSEQ Lite (v0.20.3), and low-complexity reads (DUST of >4) were removed from the BAM files. The alignment results were parsed via SAMtools to generate SAM files. Read counts to each genomic feature were obtained with the htseq-count program (v0.6.0) using the "union" option. After removing absent features (zero counts in all samples), the raw counts were then imported to R/Bioconductor package DESeq2 to identify differentially expressed genes among samples. DESeq2 normalizes counts by dividing each column of the count table (samples) by the size factor of this column. The size factor is calculated by dividing the samples by geometric means of the genes. This brings the count values to a common scale suitable for comparison. *P* values for differential expression are calculated using binomial test for differences between the base means of two conditions. These *P* values are then adjusted for multiple test correction using Benjamini-Hochberg algorithm to control the false discovery rate. We considered genes differentially expressed between two groups of samples when the DESeq2 analysis resulted in an adjusted *P* value of <0.05,

Downloaded from http://advances.sciencemag.org/ on February 24, 2021

and the fold change in gene expression was twofold. Cluster analyses including principal components analysis and hierarchical clustering were performed using standard algorithms and metrics. Hierarchical clustering was performed using complete linkage with Euclidean metric.

For analysis of ERV expression, the single-end reads that passed Illumina filters were filtered for reads aligning to tRNA, rRNA, adapter sequences, and spike-in controls. The reads were then aligned to the reference genome using TopHat (v1.4.1) and alignment results parsed via SAMtools to generate SAM files. The uniquely and multi-mapped reads were filtered from the BAM files using an MAPQ (mapping quality) of 255 to filter uniquely mapped reads. Read counts to each repeat element were obtained by mapping the multi-mapped reads to each of the repeat classes and counting alignment for each repeat class (all the steps are part of the RepEnrich pipeline). After removing absent repeat elements (zero counts in all samples), the raw counts were then imported to R/Bioconductor package EdgeR differentially expressed genes among samples. The generalized linear model method within the EdgeR package was used to identify differentially expressed genes. We considered genes differentially expressed between two groups of samples when the EdgeR analysis resulted in an adjusted P value of <0.05.

rADA supplementation

HUVECs were seeded at 5×10^5 cells per well in six-well plates and incubated for 24 hours at 37°C with 5% CO_2. Twenty-four hours after transfection with siRNA, fresh growth media containing rADA1 (Sigma, 93985) or ADA2 (R&D Systems, 7518-AD) was added to wells (50 to 1000 ng/ml). Where indicated, pentostatin (10 μM) was added 1 hour before rADA2. Seventy-two hours after transfection, cells were harvested, and gene expression was analyzed by qRT-PCR.

Coculture of HUVEC and U937

HUVECs (1.4×10^5) were plated in 24-well plates. Twenty-four hours after transfection with siRNA, media was changed into fresh EGM-2, and wild-type U937 cells (1×10^5 cells/200 μl of RPMI, 2% FBS) were plated on polyester membrane Transwell clear inserts (0.4 μm) and cocultured with HUVECs for an additional 48 hours before analysis of gene expression by qRT-PCR.

Metabolite extraction and LC-MS/MS

For cell sample preparation, 3×10^6 HUVECs were lysed by aspirating in 80% cold methanol, followed by three freeze-thaw cycles, where samples were alternated between 40° and −80°C baths in 30-s intervals. Lysates were then centrifuged at 4°C at 14,000 rpm for 10 min to remove cellular debris, and supernatants were dried using a Speed Vacuum system for 2 hours at 30°C before resuspension in an 80:20 ratio of methanol and water. For spent media samples, media was centrifuged at 14,000 rpm for 1 min to remove cell debris before adding cold methanol at a ratio of 80:20 methanol and water. Cell and media samples were placed at −20°C for 30 min to precipitate protein before centrifugation at 14,000 rpm for 10 min at 4°C. Each injection for liquid chromatography–tandem MS (LC-MS/MS) analysis was equivalent to 80,000 cells or 0.5 μl of media. LC was performed with a Vanquish UHPLC system (Thermo Fischer Scientific) using a ZIC-pHILIC polymeric column (EMD Millipore) (150 mm by 2.1 mm, 5 μm). Mobile phases used were (A) 20 mM ammonium bicarbonate in water (pH 9.6) and (B) acetonitrile. Mobile phase gradients were as follows: 90% B for first two 2 min followed by a linear gradient to 55% B at 16 min, sustained for an additional 3 min before final re-equilibration for 11 min at 90% B. Column temperature was 25°C, and mobile phase flow rate was 0.3 ml/min. Detection was performed using a Q Exactive Orbitrap mass spectrometer with heated electrospray ionization source (Thermo Scientific). Sheath and auxiliary gas were high purity nitrogen at 40 au (arbitrary units) and 20 au, respectively. MS/MS were collected in both positive and negative ionization polarities. Ion transfer tube was set at 275°C, and vaporizer temperature was set to 350°C. Collision-induced dissociation (CID) MS2 was collected using stepped normalized collision energies of 15, 30, and 45 au and isolation widths of ±0.5 mass/charge ratio (m/z). Peak heights from chromatograms corresponding to metabolites of interest were used for quantification. Indicated metabolites were detected as protonated/deprotonated ions of their monoisotopic masses, and identities were confirmed by comparison to the MS1 and MS2 patterning of known standards under this LC-MS method.

Methionine labeling and SAM flux

EGM-2 medium with dialyzed serum containing 64 μM unlabeled methionine was supplemented with either 64 μM U-^{13}C methionine (Cambridge Isotope Laboratories Inc.; ^{13}C medium) or 64 μM unlabeled methionine (^{12}C medium). At time zero, cells cultured in ^{12}C medium were switched to ^{13}C medium, incubated for 10 or 30 min at 37°C, washed twice with ice-cold phosphate-buffered saline (PBS), extracted in 80% cold methanol, and analyzed with LC-MS as described above to obtain mass isotopomer distributions. Because of lack of remethylation of homocysteine, SAM metabolism was modeled as a linear pathway from methionine to SAM to SAH, governed by the differential equations

$$\dot{x}_{SAM}/\mu_{SAM} = x_{met} - x_{SAM}$$

$$\dot{x}_{SAH}/\mu_{SAH} = x_{SAM} - x_{SAH}$$

where x_{SAM} and x_{SAH} are time-dependent mass isotopomer fractions with time derivatives $\dot{x}$, while x_{met} was considered constant; v is the flux through the linear pathway; and μ is the rate constant, related to the flux as $\mu \cdot c = v$, where c is the pool size (concentration) (*19*). This model was fit to the $^{13}C_5$-methionine, $^{13}C_5$-SAM, and $^{13}C_4$-SAH mass isotopomers at the 10- and 30-min time points by minimizing the variance-weighted sum of square errors. The resulting observed x^2 error was 3.95, which was acceptable at the 95% level. CIs for the parameters μ were obtained as previously described (*43*). Change in flux was obtained as the ratio

$$v^{siADA2}/v^{siCtrl} = \mu^{siADA2} c^{siADA2}/(\mu^{siCtrl} c^{siCtrl})$$

and 95% CIs for this ratio were obtained from the corresponding CIs for μ.

ADA and MAT activity

In vitro dAdo deamination assays were adapted from previously described methodology (*11*) by measuring de novo dIno and hypoxanthine production using LC-MS/MS. For extracellular activity, cultured HUVEC-conditioned EGM-2 supernatant was centrifuged at 1500 rpm for 5 min to remove cellular debris. For intracellular activity, whole-cell lysates were diluted to 10×10^5 cell equivalents per milliliter in cold PBS. Supernatant or lysate was incubated with

Downloaded from http://advances.sciencemag.org/ on February 24, 2021

100 nM to 1 mM isotopically labeled 2′-deoxyadenosine ($^{15}N_5$, Cambridge Isotope Laboratories) for 30 and 120 min at 37°C. Reactions were quenched using ice-cold methanol at a ratio of 80:20 methanol: reaction volume and centrifuged at 14,000 rpm for 10 min to remove protein. Supernatant was isolated, from which 2 μl was injected for LC-MS/MS analysis. Quantification of deaminase activity was measured as nanomoles of isotopically labeled dAdo and hypoxanthine produced per liter per minute. For quantification of extracellular, HUVEC-derived ADA activity, reaction rate in cell-free EGM-2 growth media was subtracted from rates in culture supernatant, and data were normalized to cell number and protein concentration. In vitro methionine adenosyl-transferase assays were performed by detection of isotopically labeled *S*-adenosyl methionine by LC-MS/MS, as described above. Fresh cytoplasmic protein lysates were isolated from U937 monocytes. In tissue culture–treated, 96-well low-evaporation plates, 10 μg of lysate was incubated with 1 mM U-^{13}C methionine, 1 mM ATP, and nucleoside at indicated concentration. Reactions were buffered in 20 mM $MgSO_4$, 150 mM KCl, and 100 mM tris (pH 7.4). After incubation for 30 min at 37°C, reactions were quenched using ice-cold methanol at a ratio of 80:20 methanol:reaction volume. Samples were centrifuged at 14,000 rpm for 10 min to remove protein, and supernatants were dried using a Speed Vacuum concentrator system for 2 hours at 30°C. Samples were resuspended in 50 μl of 80:20 methanol and water, with 2 μl injected for LC-MS/MS. Quantification of MAT activity was measured via *m/z* 404.1611 chromatogram peak intensity, corresponding to the $M+H^+$ ion of 5-carbon U-^{13}C–labeled *S*-adenosyl methionine and confirmed by diagnostic tandem mass spectra.

Quantification of labeled methyl-cytosine and labeled deoxyinosine

For labeled deoxyinosine, HUVECs were transfected with siRNA against the indicated target for 72 hours, followed by treatment with 85 μM U-^{15}N-2′-deoxyadenosine (Cambridge Isotope Laboratories) for 5 min. Cells were lysed, and metabolite extraction with LC-MS/MS was performed as described. 2′-Deoxyinosine with full label incorporation (4^{15}N-2′-deoxyinosine) was identified by diagnostic MS/MS fragmentation pattern, and relative abundance was quantified by peak height. For labeled methyl-cytosine, HUVECs were transfected with siRNA against the indicated target for 72 hours. During this time, cells were incubated with U-^{13}C methionine (Cambridge Isotope Laboratories) at 64 μM, the equivalent concentration to endogenous levels in growth medium, for the indicated times. Following lysing, genomic DNA was isolated using the PureLink Genomic DNA Mini Kit (Invitrogen) and quantified before digestion with a DNA Degradase I (Zymogen) kit according to the manufacturer's protocol. Product deoxynucleosides were mixed 1:2 with a 50% acetonitrile and 50% water and 40 mM ammonium bicarbonate solution. Each injection of digested genomic isolate was equivalent to 5 ng of DNA. LC was performed with a Vanquish UHPLC system (Thermo Scientific) using a ZIC-HILIC column (EMD Millipore) (150 mm × 1 mm, 5 μM). Metabolites were eluted following a gradient mobile phase of (A) 40 mM ammonium bicarbonate and (B) acetonitrile. The gradients were used as follows: 90% B at start, immediately following a linear gradient to 0% B over 2 min, and sustaining 0% B for two additional minutes of detection before a final equilibration for 1 min at 90% B. Column temperature was 25°C, and mobile phase flow rate was 0.175 ml/min. Detection was performed using a Q Exactve Orbitrap mass spectrometer (Thermo Scientific) as described above, with CID MS2 collected using stepped normalized collision energies of 30 and 45 au. Peak heights from chromatograms corresponding to the M+1 isotopomer of 2′-deoxy-5-methylcytidine were used for quantification, subtracting peak height attributable to naturally occurring ^{13}C isotope.

ERV cloning

cDNAs for ERVK28 transcripts 1 and 3 were ordered from IDT. cDNAs were amplified using the Phusion polymerase enzyme and specific primers that are flanked by Eco RI (forward: 5′-GCT**GAATTC**-CAGGTATTGTAGGGG-3′ for transcript 1; forward: 5′-GCT-**GAATTC**ATGAACCCATCGGAG-3′ for transcript 3; Eco RI sites in bold) and Apa I or Xho I restriction sites (reverse: 5′-GT**GGGCCC**T-GCAAAATGGAGT-3′ for transcript 1; Apa I site in bold; reverse: 5′-G**CTCGAG**GCGCAGAATTTTTC-3′ for transcript 3; Xho I site in bold), respectively. The amplicons [308 base pair (bp) for transcript 1 and 457 bp for transcript 3] were digested with Eco RI/Apa I and Eco RI/Xho I, respectively, and were cloned in frame with Flag between the Eco RI and Apa I sites or Eco RI and Xho I sites, respectively, in pcDNA3-Flag-TRAF6 (Addgene, no. 66929). Plasmids were produced in One Shot TOP10 bacteria, and constructs sequence was verified.

ERV overexpression

For electroporation, 2×10^5 HUVECs were transferred to a sterile 1.5-ml microcentrifuge tube, resuspended in 10 μl of buffer R, and mixed with 500 ng of pcDNA3-Flag vector. DNA electroporation was performed with a Neon Transfection System 10 μl kit (Thermo Fisher Scientific) using the following settings: 1350 V, 30 ms, and 2 pulses. After electroporation, cells from five 10-μl transfection reactions were added to the same well of a six-well plate containing 2 ml of prewarmed supplemented EGM-2 BulletKit growth media (Lonza) without antibiotics. Twenty-four hours after transfection, new media with antibiotics was added to the wells. Forty-eight hours after transfection, total RNA was extracted using a Quick-RNA MiniPrep Plus kit (Zymo Research). RNA (500 ng) was used to synthesize cDNA using a qScript cDNA synthesis kit (Quanta). Samples were diluted sixfold, and gene expression was analyzed on a CFX96 Touch Detection System (Bio-Rad) using TaqMan Universal PCR Master Mix (Thermo Fisher Scientific).

Statistical analysis

Data values are reported as means ± SD, with differences determined using two-tailed Student's *t* test, with Benjamini-Hochberg adjustment for multiple comparisons. Regarding statistical calculations, normal data distribution was confirmed using controls or previously generated large-scale datasets ($n > 384$) before analysis of experimental samples. All reported results were independently replicated using three independent experiments.

SUPPLEMENTARY MATERIALS

Supplementary material for this article is available at http://advances.sciencemag.org/cgi/content/full/6/30/eaba3688/DC1

View/request a protocol for this paper from *Bio-protocol*.

REFERENCES AND NOTES

1. G. R. Stark, How cells respond to interferons revisited: from early history to current complexity. *Cytokine Growth Factor Rev.* **18**, 419–423 (2007).

Downloaded from http://advances.sciencemag.org/ on February 24, 2021

2. J. Wu, Z. J. Chen, Innate immune sensing and signaling of cytosolic nucleic acids. *Annu. Rev. Immunol.* **32**, 461–488 (2014).
3. R. Dhanwani, M. Takahashi, S. Sharma, Cytosolic sensing of immuno-stimulatory DNA, the enemy within. *Curr. Opin. Immunol.* **50**, 82–87 (2018).
4. D. S. Pisetsky, The origin and properties of extracellular DNA: from PAMP to DAMP. *Clin. Immunol.* **144**, 32–40 (2012).
5. M. K. Crow, M. Olferiev, K. A. Kirou, Type I Interferons in Autoimmune Disease. *Annu. Rev. Pathol.* **14**, 369–393 (2019).
6. C.-W. Lio, B. McDonald, M. Takahashi, R. Dhanwani, N. Sharma, J. Huang, E. Pham, C. A. Benedict, S. Sharma, cGAS-STING Signaling Regulates Initial Innate Control of Cytomegalovirus Infection. *J. Virol.* **90**, 7789–7797 (2016).
7. A. Belot, E. Wassmer, M. Twilt, J. C. Lega, L. A. Zeef, A. Oojageer, P. R. Kasher, A. L. Mathieu, C. Malcus, J. Demaret, N. Fabien, S. Collardeau-Frachon, L. Mechtouff, L. Derex, T. Walzer, G. I. Rice, I. Durieu, Y. J. Crow, Mutations in CECR1 associated with a neutrophil signature in peripheral blood. *Pediatr. Rheumatol. Online J.* **12**, 44 (2014).
8. A. V. Zavialov, A. Engstrom, Human ADA2 belongs to a new family of growth factors with adenosine deaminase activity. *Biochem. J.* **391**, 51–57 (2005).
9. N. A. Andreasyan, H. L. Hairapetyan, Y. G. Sargisova, S. S. Mardanyan, ADA2 isoform of adenosine deaminase from pleural fluid. *FEBS Lett.* **579**, 643–647 (2005).
10. N. Novershtern, A. Subramanian, L. N. Lawton, R. H. Mak, W. N. Haining, M. E. McConkey, N. Habib, N. Yosef, C. Y. Chang, T. Shay, G. M. Frampton, A. C. Drake, I. Leskov, B. Nilsson, F. Preffer, D. Dombkowski, J. W. Evans, T. Liefeld, J. S. Smutko, J. Chen, N. Friedman, R. A. Young, T. R. Golub, A. Regev, B. L. Ebert, Densely interconnected transcriptional circuits control cell states in human hematopoiesis. *Cell* **144**, 296–309 (2011).
11. Q. Zhou, D. Yang, A. K. Ombrello, A. V. Zavialov, C. Toro, A. V. Zavialov, D. L. Stone, J. J. Chae, S. D. Rosenzweig, K. Bishop, K. S. Barron, H. S. Kuehn, P. Hoffmann, A. Negro, W. L. Tsai, E. W. Cowen, W. Pei, J. D. Milner, C. Silvin, T. Heller, D. T. Chin, N. J. Patronas, J. S. Barber, C. C. Lee, G. M. Wood, A. Ling, S. J. Kelly, D. E. Kleiner, J. C. Mullikin, N. J. Ganson, H. H. Kong, S. Hambleton, F. Candotti, M. M. Quezado, K. R. Calvo, H. Alao, B. K. Barham, A. Jones, J. F. Meschia, B. B. Worrall, S. E. Kasner, S. S. Rich, R. Goldbach-Mansky, M. Abinun, E. Chalom, A. C. Gotte, M. Punaro, V. Pascual, J. W. Verbsky, T. R. Torgerson, N. G. Singer, T. R. Gershon, S. Ozen, O. Karadag, T. A. Fleisher, E. F. Remmers, S. M. Burgess, S. L. Moir, M. Gadina, R. Sood, M. S. Hershfield, M. Boehm, D. L. Kastner, I. Aksentijevich, Early-onset stroke and vasculopathy associated with mutations in ADA2. *N. Engl. J. Med.* **370**, 911–920 (2014).
12. A. V. Zavialov, X. Yu, D. Spillmann, G. Lauvau, A. V. Zavialov, Structural basis for the growth factor activity of human adenosine deaminase ADA2. *J. Biol. Chem.* **285**, 12367–12377 (2010).
13. P. Y. Lee, Z. Huang, M. S. Hershfield, P. A. Nigrovic, Analysis of peripheral blood ADA1 and ADA2 levels in children and adults. Response to: 'Total adenosine deaminase highly correlated with adenosine deaminase 2 activity in serum' by Gao et al. *Ann. Rheum. Dis.* annrheumdis-2020-217055 (2020).
14. J. Linden, F. Koch-Nolte, G. Dahl, Purine Release, Metabolism, and Signaling in the Inflammatory Response. *Annu. Rev. Immunol.* **37**, 325–347 (2019).
15. E. Szabados, R. G. Duggleby, R. I. Christopherson, Metabolism of adenosine and deoxyadenosine by human erythrocytes and CCRF-CEM leukemia cells. *Int. J. Biochem. Cell Biol.* **28**, 1405–1415 (1996).
16. R. T. Smolenski, Z. Kochan, R. McDouall, A. M. Seymour, M. H. Yacoub, Adenosine uptake and metabolism in human endothelial cells. *Adv. Exp. Med. Biol.* **370**, 435–438 (1994).
17. M. Jain, R. Nilsson, S. Sharma, N. Madhusudhan, T. Kitami, A. L. Souza, R. Kafri, M. W. Kirschner, C. B. Clish, V. K. Mootha, Metabolite profiling identifies a key role for glycine in rapid cancer cell proliferation. *Science* **336**, 1040–1044 (2012).
18. R. L. Williams-Karnesky, U. S. Sandau, T. A. Lusardi, N. K. Lytle, J. M. Farrell, E. M. Pritchard, D. L. Kaplan, D. Boison, Epigenetic changes induced by adenosine augmentation therapy prevent epileptogenesis. *J. Clin. Invest.* **123**, 3552–3563 (2013).
19. R. Nilsson, M. Jain, Simultaneous tracing of carbon and nitrogen isotopes in human cells. *Mol. BioSyst.* **12**, 1929–1937 (2016).
20. L. Huang, D. Kim, X. Liu, C. R. Myers, J. W. Locasale, Estimating relative changes of metabolic fluxes. *PLOS Comput. Biol.* **10**, e1003958 (2014).
21. K. B. Chiappinelli, P. L. Strissel, A. Desrichard, H. Li, C. Henke, B. Akman, A. Hein, N. S. Rote, L. M. Cope, A. Snyder, V. Makarov, S. Budhu, D. J. Slamon, J. D. Wolchok, D. M. Pardoll, M. W. Beckmann, C. A. Zahnow, T. Merghoub, T. A. Chan, S. B. Baylin, R. Strick, Inhibiting DNA Methylation Causes an Interferon Response in Cancer via dsRNA Including Endogenous Retroviruses. *Cell* **164**, 1073 (2016).
22. I. Canadas, R. Thummalapalli, J. W. Kim, S. Kitajima, R. W. Jenkins, C. L. Christensen, M. Campisi, Y. Kuang, Y. Zhang, E. Gjini, G. Zhang, T. Tian, D. R. Sen, D. Miao, Y. Imamura, T. Thai, B. Piel, H. Terai, A. R. Aref, T. Hagan, S. Koyama, M. Watanabe, H. Baba, A. E. Adeni, C. A. Lydon, P. Tamayo, Z. Wei, M. Herlyn, T. U. Barbie, R. Uppaluri, L. M. Sholl, E. Sicinska, J. Sands, S. Rodig, K. K. Wong, C. P. Paweletz, H. Watanabe, D. A. Barbie, Tumor innate immunity primed by specific interferon-stimulated endogenous retroviruses. *Nat. Med.* **24**, 1143–1150 (2018).
23. Z.-W. Gao, X. Wang, F. Lin, K. Dong, Total adenosine deaminase highly correlated with adenosine deaminase 2 activity in serum. *Ann. Rheum. Dis.* annrheumdis-2020-217055 (2020).
24. I. Khodadadi, M. Abdi, A. Ahmadi, M. S. Wahedi, S. Menbari, F. Lahoorpour, R. Rahbari, Analysis of serum adenosine deaminase (ADA) and ADA1 and ADA2 isoenzyme activities in HIV positive and HIV-HBV co-infected patients. *Clin. Biochem.* **44**, 980–983 (2011).
25. E. Fernandez, L. Rodrigo, S. Riestra, S. Carcia, F. Gutierrez, G. Ocio, Adenosine deaminase isoenzymes and neopterin in liver cirrhosis. *J. Clin. Gastroenterol.* **30**, 181–186 (2000).
26. S. Valadbeigi, R. Saghiri, M. Ebrahimi-Rad, S. Khatami, H. Akhbari, Adenosine Deaminase Activity and HLA-DRB as Diagnostic Markers for Rheumatoid Arthritis. *Curr. Rheumatol. Rev.* **15**, 44–49 (2019).
27. J. P. Ungerer, H. M. Oosthuizen, J. H. Retief, S. H. Bissbort, Significance of adenosine deaminase activity and its isoenzymes in tuberculous effusions. *Chest* **106**, 33–37 (1994).
28. S. Iwaki-Egawa, T. Yamamoto, Y. Watanabe, Human plasma adenosine deaminase 2 is secreted by activated monocytes. *Biol. Chem.* **387**, 319–321 (2006).
29. N. Dale, B. G. Frenguelli, Release of adenosine and ATP during ischemia and epilepsy. *Curr. Neuropharmacol.* **7**, 160–179 (2009).
30. A. Sollevi, Cardiovascular effects of adenosine in man; possible clinical implications. *Prog. Neurobiol.* **27**, 319–349 (1986).
31. A. Surendran, M. Aliani, A. Ravandi, Metabolomic characterization of myocardial ischemia-reperfusion injury in ST-segment elevation myocardial infarction patients undergoing percutaneous coronary intervention. *Sci. Rep.* **9**, 11742 (2019).
32. A. McDonough, R. V. Lee, S. Noor, C. Lee, T. Le, M. Iorga, J. L. H. Phillips, S. Murphy, T. Moller, J. R. Weinstein, Ischemia/Reperfusion Induces Interferon-Stimulated Gene Expression in Microglia. *J. Neurosci.* **37**, 8292–8308 (2017).
33. P. Vaupel, A. Mayer, Hypoxia-Driven Adenosine Accumulation: A Crucial Microenvironmental Factor Promoting Tumor Progression. *Adv. Exp. Med. Biol.* **876**, 177–183 (2016).
34. P. A. Keyel, Dnases in health and disease. *Dev. Biol.* **429**, 1–11 (2017).
35. C. Carmona-Rivera, S. S. Khaznadar, K. W. Shwin, J. A. Irizarry-Caro, L. J. O'Neil, Y. Liu, K. A. Jacobson, A. K. Ombrello, D. L. Stone, W. L. Tsai, D. L. Kastner, I. Aksentijevich, M. J. Kaplan, P. C. Grayson, Deficiency of adenosine deaminase 2 triggers adenosine-mediated NETosis and TNF production in patients with DADA2. *Blood* **134**, 395–406 (2019).
36. B. J. Barnes, J. M. Adrover, A. Baxter-Stoltzfus, A. Borczuk, J. Cools-Lartigue, J. M. Crawford, J. Dassler-Plenker, P. Guerci, C. Huynh, J. S. Knight, M. Loda, M. R. Looney, F. McAllister, R. Rayes, S. Renaud, S. Rousseau, S. Salvatore, R. E. Schwartz, J. D. Spicer, C. C. Yost, A. Weber, Y. Zuo, M. Egeblad, Targeting potential drivers of COVID-19: Neutrophil extracellular traps. *J. Exp. Med.* **217**, e20200652 (2020).
37. P. Navon Elkan, S. B. Pierce, R. Segel, T. Walsh, J. Barash, S. Padeh, A. Zlotogorski, Y. Berkun, J. J. Press, M. Mukamel, I. Voth, P. J. Hashkes, L. Harel, V. Hoffer, E. Ling, F. Yalcinkaya, O. Kasapcopur, M. K. Lee, R. E. Klevit, P. Renbaum, A. Weinberg-Shukron, E. F. Sener, B. Schormair, S. Zeligson, D. Marek-Yagel, T. M. Strom, M. Shohat, A. Singer, A. Rubinow, E. Pras, J. Winkelmann, M. Tekin, Y. Anikster, M. C. King, E. Levy-Lahad, Mutant adenosine deaminase 2 in a polyarteritis nodosa vasculopathy. *N. Engl. J. Med.* **370**, 921–931 (2014).
38. M. L. Markert, Purine nucleoside phosphorylase deficiency. *Immunodefic. Rev.* **3**, 45–81 (1991).
39. Y. Ghodke-Puranik, J. M. Dorschner, D. M. Vsetecka, S. Amin, A. Makol, F. Ernste, T. Osborn, K. Moder, V. Chowdhary, E. Eliopoulos, M. I. Zervou, G. N. Goulielmos, M. A. Jensen, T. B. Niewold, Lupus-Associated Functional Polymorphism in PNP Causes Cell Cycle Abnormalities and Interferon Pathway Activation in Human Immune Cells. *Arthritis Rheumatol.* **69**, 2328–2337 (2017).
40. A. K. Ombrello, J. Qin, P. M. Hoffmann, P. Kumar, D. Stone, A. Jones, T. Romeo, B. Barham, G. Pinto-Patarroyo, C. Toro, A. Soldatos, Q. Zhou, N. Deuitch, I. Aksentijevich, S. L. Sheldon, S. Kelly, A. Man, K. Barron, M. Hershfield, W. A. Flegel, D. L. Kastner, Treatment Strategies for Deficiency of Adenosine Deaminase 2. *N. Engl. J. Med.* **380**, 1582–1584 (2019).
41. A. Yarilina, L. B. Ivashkiv, Type I interferon: a new player in TNF signaling. *Curr. Dir. Autoimmun.* **11**, 94–104 (2010).
42. N. Wang, H. Liang, K. Zen, Molecular mechanisms that influence the macrophage m1-m2 polarization balance. *Front. Immunol.* **5**, 614 (2014).
43. M. R. Antoniewicz, J. K. Kelleher, G. Stephanopoulos, Determination of confidence intervals of metabolic fluxes estimated from stable isotope measurements. *Metab. Eng.* **8**, 324–337 (2006).

Acknowledgments: We thank D. Araujo for editing and formatting the manuscript; Y. Kushnareva and C. Oh at the LJI Functional Genomics Center for screening; J. Huang for optimization of IRF3/IFNβ assays in primary human endothelial cells; D. Freeman, B. McDonald, and R. El Morabiti for hCMV propagation and infections; J. Day for RNA-seq; K. Lehman for metabolomics; G. Guzzo for optimization of SAM flux; J. Greenbaum and the LJI Bioinformatics

Downloaded from http://advances.sciencemag.org/ on February 24, 2021

Core for statistical analyses; and E. Chambers and the DADA2 Foundation for helpful discussions. **Funding:** This work was supported by NIH grants R01CA199376 and U01DE028227 and a research grant from the Vasculitis Foundation awarded to S.S., NIH S10OD020025 and R01ES027595 to M.J., and RO1 AI101423 to C.A.B. I.T.M. is supported by NIH T32GM007752, F31CA236405, and a SPARK award from the LJI Board of Directors. **Author contributions:** The functional screen was optimized and performed by R.D. who validated ADA2 and purine nucleosides as regulators of IFNβ in endothelial cells and monocytes. M.T. contributed significantly in defining the specific mechanism linking ADA2 and IFNβ by designing, optimizing, and performing in vitro experiments. I.T.M. performed MS metabolomics. C.L. performed rescue experiments using rADA2 and rADA1 and ERV cloning and overexpression. A.R. performed ADA2 Western blot. J.D.W. optimized the labeled methyl-cytosine assay. B.P. compiled the list of disease genes. S.S. provided overall direction and supervised project planning and execution, with input from C.A.B. (hCMV), C.C.H. (endothelial and monocyte biology), J.L. (purine signaling), R.N. (SAM flux), and M.J. (metabolomics). S.S., M.J., R.D., M.T., and I.T.M. wrote the manuscript with input from co-authors. **Competing interests:** S.S., R.D., and M.T. are inventors on a patent application related to this work filed by La Jolla Institute for Immunology (no. US2019/0282580 A1, filed 19 September 2019). The authors declare that they have no other competing interests. **Data and materials availability:** All materials used in this study will be made available to the scientific research community, conditional upon execution of a materials transfer agreement between LJI and the recipient institution. All data needed to evaluate the conclusions in the paper are present in the paper and/or the Supplementary Materials. Raw RNA-seq data for Figs. 1D and 3D can be accessed at the Gene Expression Omnibus (GSE150540 and sGSE151924). Additional data related to this paper may be requested from the authors.

Submitted 27 November 2019
Accepted 9 June 2020
Published 22 July 2020
10.1126/sciadv.aba3688

Citation: R. Dhanwani, M. Takahashi, I. T. Mathews, C. Lenzi, A. Romanov, J. D. Watrous, B. Pieters, C. C. Hedrick, C. A. Benedict, J. Linden, R. Nilsson, M. Jain, S. Sharma, Cellular sensing of extracellular purine nucleosides triggers an innate IFN-β response. *Sci. Adv.* **6**, eaba3688 (2020).

Downloaded from http://advances.sciencemag.org/ on February 24, 2021

ScienceAdvances

Cellular sensing of extracellular purine nucleosides triggers an innate IFN-β response

Rekha Dhanwani, Mariko Takahashi, Ian T. Mathews, Camille Lenzi, Artem Romanov, Jeramie D. Watrous, Bartijn Pieters, Catherine C. Hedrick, Chris A. Benedict, Joel Linden, Roland Nilsson, Mohit Jain and Sonia Sharma

Sci Adv **6** (30), eaba3688.
DOI: 10.1126/sciadv.aba3688

ARTICLE TOOLS http://advances.sciencemag.org/content/6/30/eaba3688

SUPPLEMENTARY MATERIALS http://advances.sciencemag.org/content/suppl/2020/07/20/6.30.eaba3688.DC1

REFERENCES This article cites 41 articles, 6 of which you can access for free
http://advances.sciencemag.org/content/6/30/eaba3688#BIBL

PERMISSIONS http://www.sciencemag.org/help/reprints-and-permissions

Use of this article is subject to the Terms of Service

Science Advances (ISSN 2375-2548) is published by the American Association for the Advancement of Science, 1200 New York Avenue NW, Washington, DC 20005. The title *Science Advances* is a registered trademark of AAAS.

Copyright © 2020 The Authors, some rights reserved; exclusive licensee American Association for the Advancement of Science. No claim to original U.S. Government Works. Distributed under a Creative Commons Attribution NonCommercial License 4.0 (CC BY-NC).

Downloaded from http://advances.sciencemag.org/ on February 24, 2021